Ion-sensing properties of ferrocenyl-diaminomaleonitrile derivatives

A THESIS
SUBMITTED TO THE FACULTY OF THE GRADUATE SCHOOL
OF THE UNIVERSITY OF MINNESOTA
BY

Michael Raymond Dahlby

IN PARTIAL FULFILLMENT OF THE REQUIREMENTS
FOR THE DEGREE OF
MASTER OF SCIENCE

Advised by Dr. Victor Nemykin

July 2010

Acknowledgements

I would first like to thank my advisor, Dr. Victor Nemykin, whose enthusiasm never let a dull moment pass in lab. Also Dr. Steve Berry, who was very supportive in mentoring my first research opportunity. Greg Rohde contributed to the synthesis and computational work and James Muriithi aided in collecting absorption data. Pavlo Solnstev helped with the X-ray section, and offered many insightful discussions. Lastly, I would like to thank the UMD Chemistry Department for its support and the National Science Foundation (CHE-0809203) for funding.

For Mom, Paul, Gr'ma and Papa

Abstract

Mono- (**1**) and bis (**2**) -substituted Shiff bases obtained by the reaction between ferrocenecarbaldehyde and diaminomaleonitrile were prepared and characterized by ^{1}H and ^{13}C NMR, IR, UV-vis spectroscopy methods, elemental analysis, and X-ray crystallography. Electrochemical techniques were employed to investigate the possibility of a mixed-valence state of the iron centers in **2**, which are connected by a conjugated π-system. Two reversible oxidation potentials were observed in cyclic voltammetry, and spectroelectrochemical experiments revealed the presence of low-energy inter-valence charge transfer band in $\mathbf{2}^{+}$, corresponding to a weakly-coupled class II system. Both complexes were tested for cation-recognition properties using a variety of main group and transition-metal cations. It was shown that the complex **1** can be used as a selective optical sensor in recognition of Hg(II) and Ag(I) ions.

Table of Contents

List of Figures

List of Tables

List of Schemes

1. Introduction

1.1 Ferrocene History and Impact

The chemistry of ferrocene has a remarkable history. While the very first report of its synthesis appeared in an article by Kealy and Pauson in *Nature* in 1951,[1] it is widely acknowledged to have been first developed by Miller, Tebboth and Tremaine, whose report was submitted for publication first but printed several months later.[2] Interestingly, the very first synthesis of the compound may actually have been inside iron pipes used to transport cyclopentadiene, which became clogged with a substance that was later found to be ferrocene.[3] From the first reports of its synthesis it was immediately recognized to be a special kind of molecule, as it was widely believed that bonds between transition metals and hydrocarbons were always unstable. Furthermore, its unprecedented stability in high pressure, heat, and acidic conditions was explained by two independent publications suggesting a "sandwich"-type complex with aromatic properties.[4] The synthesis and characterization of ferrocene led to the successful development of a wealth of other metallocenes, and hence the field of organometallic chemistry was born.

As in the case for very few molecules, interest in this novel compound ceased to fade after its basic properties and reactivity had been fully documented. In fact, the number of articles published per year involving ferrocene has tripled over the past 20 years.[5] It has been employed in a wide range of disciplines, including catalysis, coordination chemistry, molecular devices, and even medicinal chemistry. With such a vast number of applications, it is very unlikely that interest in ferrocene-containing

compounds will dissipate any time soon, as its incorporation in these areas continues to produce practical and interesting results.

1.2 Mercury Toxicity

The presence of mercury is ubiquitous and its dangers incessant; it is a common element with many sources and is toxic in all its forms. The health risks associated with mercury contact vary depending on its form and type of exposure.[6-8] Elemental mercury itself is typically not acutely toxic unless its fumes are inhaled. If ingested, it is limited in its ability to pass into the bloodstream through the gastro-intestinal tract, but can readily do so through the lungs. Once there, it is able to penetrate the blood brain barrier, where it can wreak havoc on the central nervous system. Inorganic mercury, typically found in the divalent state, cannot cross the blood brain barrier and is therefore considered "less" toxic. However, once in the blood stream it accumulates in and causes damage to the kidneys. Organic mercury, most often in the form of monomethylmercury (CH_3Hg^+), the most common source of mercury poisoning in humans, is easily absorbed through the intestinal tract. It too can pass the blood brain barrier and it gained infamy after it was discovered to be the cause of Minimata disease. For these reasons, mercury is considered one of the most toxic elements.

Surprisingly, for being such a toxic element, the causes of mercury contamination in the environment include a plethora of sources, both natural and anthropogenic. As a transition metal, it is a natural component of the Earth's crust, found mainly in the form of cinnabar (HgS).[9] Other natural sources of mercury include volcanic and other geothermal activity,[10] forest fires,[11] and oceanic emissions. These natural sources,

however, are diminutive in comparison to anthropogenic sources. Combustion of fossil fuels was found to be the largest source of environmental mercury in a study published by the EPA in 1997.[12]

The dangers of mercury contamination are compounded by its complex environmental cycle. Mercury is constantly being oxidized, reduced, and methylated in the environment and is often deposited in locations far from its original source. Microorganisms in aquatic environments are able to convert inorganic mercury to methylmercury, which biomagnifies as it pervades the food chain. As in Minimata, the result of this process is the potential of lethal amounts of mercury becoming prevalent at the top of the food chain.

1.3 Mercury Detection and Chemosensors

Because its presence is so widespread, an equally diverse number of methods have been developed to detect mercury in its various forms. Some examples include the detection of elemental mercury in the exhaust of coal combustion,[13] bacterial sensor for organic mercury compounds,[14] and inductively coupled plasma in tracing mercury sources by its isotopic ratios.[15] Most research involving the detection of divalent mercury focuses on the use of molecular devices, or chemosensors.

The term chemosensor broadly refers to a class of compounds or molecular assemblies capable of detecting the presence of an analyte. The chemosensor operates via two intrinsic properties; first, the chemosensor must act as a host or receptor, having the capacity to bind to the guest through intermolecular forces, i.e. dipole-dipole, hydrogen bonding, π-π interactions, etc. Second, the binding event must elicit some measurable

change in the physical properties of the chemosensor. Changes in absorption, fluorescence, or redox potential are ideal methods of detection due to the relative ease with which samples can be prepared and data obtained. Due to the multitude of interactions capable of inducing measurable effects, a wide array of chemosensors have been developed for various guest species, including cations (copper,[16] lead,[17] iron,[18] and other transition metals), anions (fluoride,[19] cyanide,[20] etc.), and larger molecules (amino acids,[21] ATP,[22]).

Because it is a soft acid, chemosensors showing selectivity for Hg^{2+} often incorporate various soft donor atoms including sulfur, nitrogen, and phosphorous. Optical sensing, via fluorescence and/or absorbance response, offers the most attractive method for the detection of Hg^{2+}. Both types of sensors have advantages. Fluorescent sensors based on BODIPY[23] and rhodamine[24] derivatives have been shown useful for in vivo detection of Hg^{2+}. A wealth of other chemosensors has shown fluorescent sensitivity toward Hg^{2+}, either by quenching of the signal or its enhancement. Several examples are based on other rhodamine dyes,[25] crown ethers,[26] and coumarin derivatives.[27] While useful for detection within cells, this method is not conducive to immediate testing for environmental contamination. For this purpose, it is of advantage to be able to detect the presence of Hg^{2+} by the naked eye, thus eliminating the need for any instrumentation. Previous examples of such optically sensitive chemosensors also include some rhodamine[28] and crown ether[29] derivatives and hemicyanine dyes.[30]

Additionally, the incorporation of an active redox center may allow for an electrochemical response. Ferrocene is an attractive tool for this purpose due to its stable,

active redox center and its ability to withstand harsh synthetic procedures. It has been employed succesfully in a large variety chemosensors, including calcium,[31] mercury,[32] and thrombin[33] sensors.

1.4 Mixed Valence Ferrocenes

Mixed-valence ions have been a subject of interest since the late 1960's when papers published by Robin and Day as well as Marcus and Hush set the backround for discussions about mixed-valence compounds. The Robin and Day classification scheme[34] is used profusely in the literature to describe the level of delocalization between the centers of mixed-valence compounds. Class I compounds consist of two centers in which the electron is localized at one center with zero delocalization. Compounds of this class maintain the properties of the respective oxidation states of the metal centers (*i.e.* Fe^{2+}/Fe^{3+}). The opposite of this is class III, where the electron is completely delocalized between the metal centers (*i.e.* $Fe^{2.5+}/Fe^{2.5+}$). Class II compounds exhibit some degree of delocalization while maintaining the properties of the isolated oxidation centers. This class of mixed-valence compounds has inter-valence charge transfer (IVCT) processes.[35]

There are several techniques used in determining the degree of delocalization observed in mixed-valence compounds. Qualitatively, peak separation in electrochemical voltammograms may give some clue as to the amount of delocalization.[36] Larger separation between redox potentials involves a higher degree of delocalization, as no interaction results in the two iron centers exhibiting the same redox potentials. Hush theory allows for a more quantitative determination of delocalization. The parameters H_{ab}

(electronic coupling parameter) and α (delocalization parameter) allow for the calculation of the extent of delocalization from experimental absorption spectra by the equations:

$$H_{ab} = 2.06 \times 10^{-2} (\varepsilon_{max} \nu_{max} \Delta\nu_{1/2})^{1/2} / (br) \qquad (1)$$

$$\alpha^2 = 4.2 \times 10^{-4} \varepsilon_{max} \Delta\nu_{1/2} / (b \nu_{max} r^2) \qquad (2)$$

where ε_{max} is the molar absorption coefficient of the inter-valence charge transfer (IVCT) band, ν_{max} is the energy of the IVCT band (cm^{-1}), $\Delta\nu_{1/2}$ is the bandwidth at half-height of the IVCT band (cm^{-1}), *b* is the degeneracy of the transition, and *r* is the distance between centers (Å). The value H_{ab} corresponds to the electronic coupling parameter. It is equal to zero for class I compounds and quite large for class III. The calculation with formula (1) only provides a lower limit of H_{ab}, however, as it does not account for possible solvation effects and actual charge-transfer distance.[37] The value α corresponds to the degree of delocalization. It takes on values of ~0 in the case of class I and 0.707 for class III.[38] Class II compounds take on values anywhere between.

Directly-linked ferrocene compounds were first examples of the mixed-valence organometallic compounds. Cowan and Kaufman reported in 1970 the presence of an absorption band in the near-IR region (1900 nm) in the monocation biferrocene picrate salt, which was not present in the neutral biferrocene spectrum nor in the dication.[39] The Fe-Fe distance is 3.8 – 5.1 Å, depending on the cis/trans configuration, and the mixed-valence communication was thus attributed to metal orbital overlap and later confirmed by the lack of an IVCT band in selenium-linked biferrocene (little metal-metal overlap, Fe-Fe distance = 6.06 Å), while the boron-linked species did show IVCT (more metal-metal overlap, Fe-Fe distance = 5.36 Å).[40] In 1974, diferrocenylacetylene was shown to

be the first example of a bridged biferrocene exhibiting an IVCT band. Due to the estimated Fe – Fe distance of 6.5 – 7.3 Å being too great for direct metal orbital overlap, it was shown that the electron transfer must occur through the π-orbitals of the bridging ligand.

1.5 Project Overview

The work reported here is on the condensation products of ferrocene carbaldehyde and diaminomaleonitrile (DAMN). A previously published report on these compounds describes their nonlinear optical properties.[41] No information, however, can be found on the structural, optical, or electrochemical properties of these compounds and thus these properties form the basis of this work. Consequently, these compounds have been found to yield interesting properties applicable to the fields of chemosensing and mixed-valence compounds.

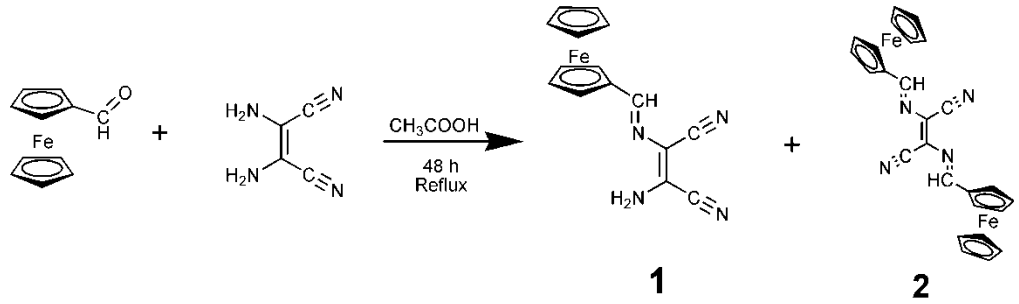

Scheme 3. Synthesis of ferrocenyl-containing Schiff base maleonitrile and fumaronitrile derivatives.

2. Experimental Section

2.1 Materials

All solvents and reagents were purchased from commercial sources and used without further purification except for dry dichloromethane which was obtained from an MBraun solvent purification system. For electrochemical experiments, tetrabutylammonium tetrakis(pentafluorophenyl)borate (TFAB) was prepared according to the literature.[42] Silica gel (60 Å, 63-100 μm) was purchased from Dynamic Adsorbents.

2.2 Synthesis

Ferrocene carbaldehyde (8.91 g, 41.6 mmol, 3 eq.) was added to 100 mL of glacial acetic acid and stirred until completely dissolved. Diaminomaleonitrile (1.51 g, 14.0 mmol, 1 eq.) was then added to the reaction mixture in one portion. This solution was stirred for 48 h and refluxed daily. TLC (silica, chloroform) of the reaction solution revealed four distinct bands: dark blue, violet, orange, and red. The reaction mixture was quenched with aqueous sodium chloride solution, resulting in a black clumpy precipitate. This crude product was collected via a fine grade filter funnel, washed several times with distilled water, and dried. TLC (silica, chloroform) showed overlapping purple, green, and orange bands surrounded by distinct blue and red bands. The products were separated by column chromatography using silica gel and triethylamine/chloroform (1:99) as the eluent. The first dark blue fraction was collected and dried under reduced pressure to yield pure sample of **2**. ^{1}H NMR (500 MHz, $CDCl_3$, TMS), δ(ppm) = 4.28 (s, 10H, Cp-

H), 4.72 (t, 4H, J = 1.95 Hz, β-Cp), 4.91 (t, 4H, J = 1.95 Hz, α-Cp), 8.76 (s, 2H, CH=N). ^{13}C NMR (125 MHz, $CDCl_3$, TMS), δ(ppm) = 68.27 (β-Cp), 70.18 (Cp), 74.04 (α-Cp), 79.41 (*i*-Cp), 111.52, 129.70 (CN, C=C), 166.64 (C=N)**.** IR(KBr, cm^{-1}): 3114, 2363, 2345, 2212 (CN), 1578 (C=N, C=C), 1400, 1370, 1260, 1210, 1156, 1105, 1043. Anal. Calc. (found): C 62.43 (62.33), H 4.04 (4.77), N 11.20 (8.92). The last fraction, dark red in color, was collected, dried under reduced pressure, and rinsed with hexanes to yield **1**. ^{1}H NMR (500 MHz, $CDCl_3$, TMS), δ(ppm) = 4.23 (s, 5H, Cp-H), 4.60 (s, 2H, β-Cp), 4.74 (s, 2H, α-Cp), 4.92 (s, 2H, NH_2), 8.37 (s, 1H, CH=N). ^{13}C NMR (125 MHz, $CDCl_3$, TMS), δ(ppm) = 69.39, 69.82, 72.59, 79.06 (Cp), 109.66, 112.60, 114.17, 121.92 (CN, C=C), 161.52 (C=N). IR = 3428, 3320 (NH_2), 3157, 3092, 2230 (CN), 2199 (CN), 1602 (C=N, C=C), 1474, 1376, 1328, 1256, 1104, 1043. Anal. Calc. (found): C 59.23 (58.23), H 3.98 (3.83), N 18.42 (17.00).

2.3 Instrumentation

NMR spectra were obtained using a Varian Unity INOVA instrument at 500 MHz for proton and 125 MHz for carbon at 25°C. Infrared spectra were obtained in KBr pellets using a Perkin Elmer Spectrum BX FT-IR system. UV-Vis spectra were recorded on a Jasco V-670 spectrophotometer at room temperature. Electrochemical data were collected with a CH Instruments CHI620C electrochemical analyzer with a three-electrode scheme and platinum electrodes. Spectroelectrochemical data were obtained using a custom-made quartz cell with a platinum mesh working electrode. Elemental analysis was performed by Atlantic Microlab, Inc. in Atlanta. Calculations were performed using Gaussian03 software package.[43] Gas-phase geometries were optimized ab-initio at DFT level with the

BP86 exchange-correlation functional using Wachter's full electron basis set for iron and the 6-311G(d) basis set for carbon, nitrogen, and hydrogen. Optimized geometries were confirmed by the positive energies of all predicted vibrations. Molecular orbital contributions were compiled from single point calculations using the VMOdes program.[44] Excitation energies were calculated at the TDDFT level for the first 30 states

X-ray Crystallography. X-ray quality single crystals of **1** and **2** were obtained by slow evaporation of corresponding dichloromethane solutions. Experimental data for **1** were collected using Rigaku Rapid II X-ray diffractometer with curved IPDS detector using graphite-monochromatized Mo-K_α radiation (λ = 0.71075 Å). Rigaku AFC-7R four-circle X-ray diffractometer with point detector using graphite-monochromatized Mo-K_α radiation (λ = 0.71069 Å) was used for X-ray structure determination of **2**. Both structures were solved by direct method implemented in to SIR-92 program and expanded using Fourier techniques. All non hydrogen atoms were refined in anisotropic approximation by Full-matrix least square method based on F^2 implemented into SHELXL software for **1** and CRYSTALS software for **2**. C-H hydrogen atoms were located from difference Fourier map and refined in the riding model approximation (U^H = $1.2U_{eq}^C$, U_{eq} = ⅓(U_{11}+U_{22}+U_{33})). For **1** hydrogen atoms of amino group were found from difference Fourier map and their coordinates were left to be refined but displacement parameters were bound to those of parent atom (U^H = $1.5U_{eq}^N$). ORTEP -3 for Windows software was used for visualization of results. All information about the refinement of crystal structures is presented in Table 1 below and corresponding CIF files are presented in the Supplemental Section.

3. Results

3.1 Synthesis

The synthesis of Schiff bases from an aldehyde and primary amine proceeds first by nucleophilic attack of the amine on the aldehyde, followed by condensation to form the carbon-nitrogen double bond (Scheme 2). The reaction should be favored in acidic media, with a proton being attracted to the lone pairs on the carbonyl oxygen, thus creating more partial positive charge on the elecrophilic carbon. However, low yields of the target compounds (<10%) were obtained. Since the final products were obtained from

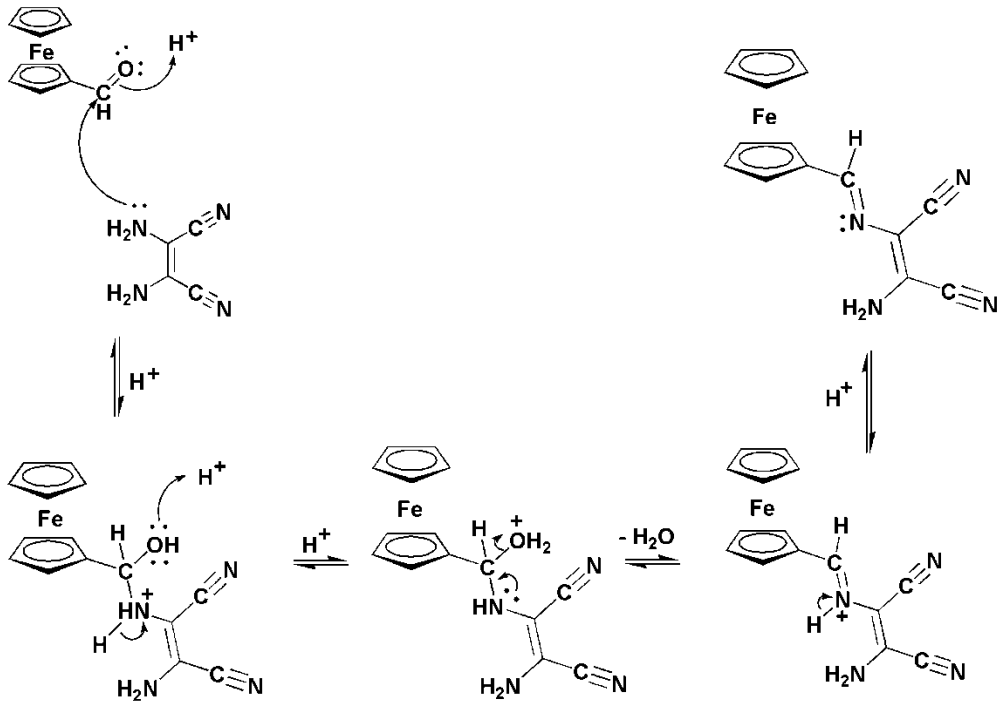

Scheme 4. General mechanism of acid-catalyzed condensation as applied to Scheme 1.

the elimination of water, it was thought that the presence of a drying agent would help push the reaction towards the products. A small amount of magnesium sulfate was added halfway through the allotted reaction time. This did not, however, significantly improve the percent yield of the target compounds. Future strategies to improve the yield of this reaction may include the use of other protic solvents with a catalytic amount of strong acid, alternate strategies for removal of water, with or without an inert atmosphere.

3.2 NMR Spectra

In the case of unsubstituted ferrocene, all ten hydrogens appear as one signal because they are all in the same environment. Upon addition of a single substituent, this symmetry is broken. The cyclopentadienyl ring containing the subsituent loses a proton and the remaining four protons appear as two signals in accordance with their proximity to the substituent. The protons closest to the substituent are typically given the alpha (α) designation, and those further from the substituent are designated as beta (β) protons. The protons of the unsubstituted cyclopentadienyl ring maintain their equivalency and appear as one signal and given the "Cp-H" designation. The result is a 5:2:2 ratio of peaks for a mono-substituted ferrocene unit. Both products **1** and **2** contain this signature set of peaks in their ^{1}H NMR spectra. Compound **1** (Figure 1) has chemical shifts of 4.23 (Cp-H), 4.60 (α-Cp), and 4.74 (β-Cp) ppm with respect to the tetramethylsilane (TMS) standard. Compound **2** has shifts of 4.28 (Cp-H), 4.72 (α-Cp), and 4.91 (β-Cp) ppm. Due to the presence of two ferrocene units, the ratios are 10:4:4. The α-Cp and β-Cp of **2** (Figure 2) were observed as triplets, with a coupling constant of J = 1.95 Hz. The amine

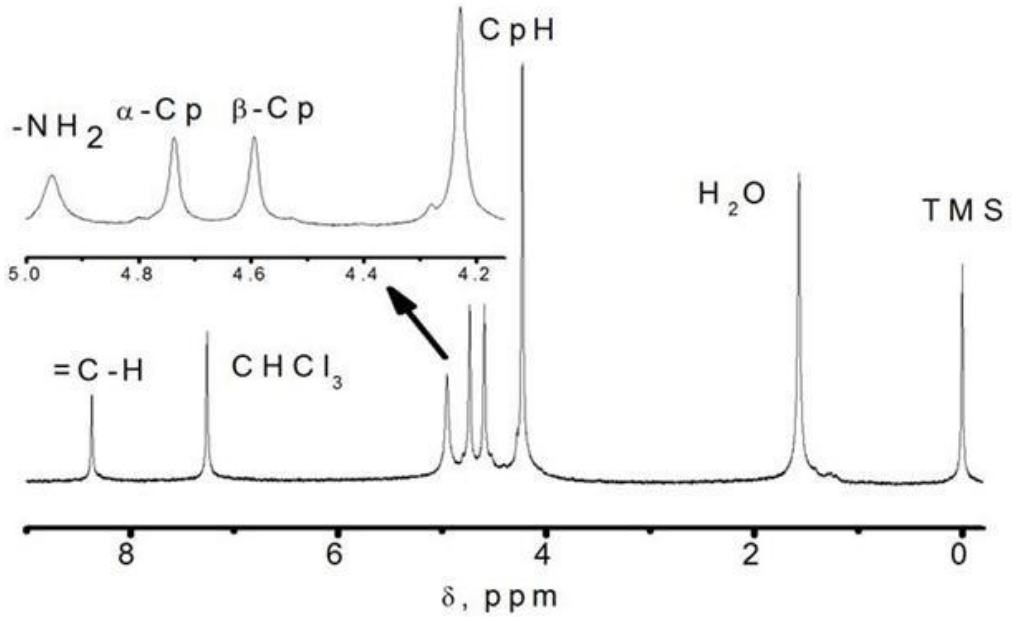

Figure 1. ^{1}H NMR spectrum of **1** in $CDCl_3$.

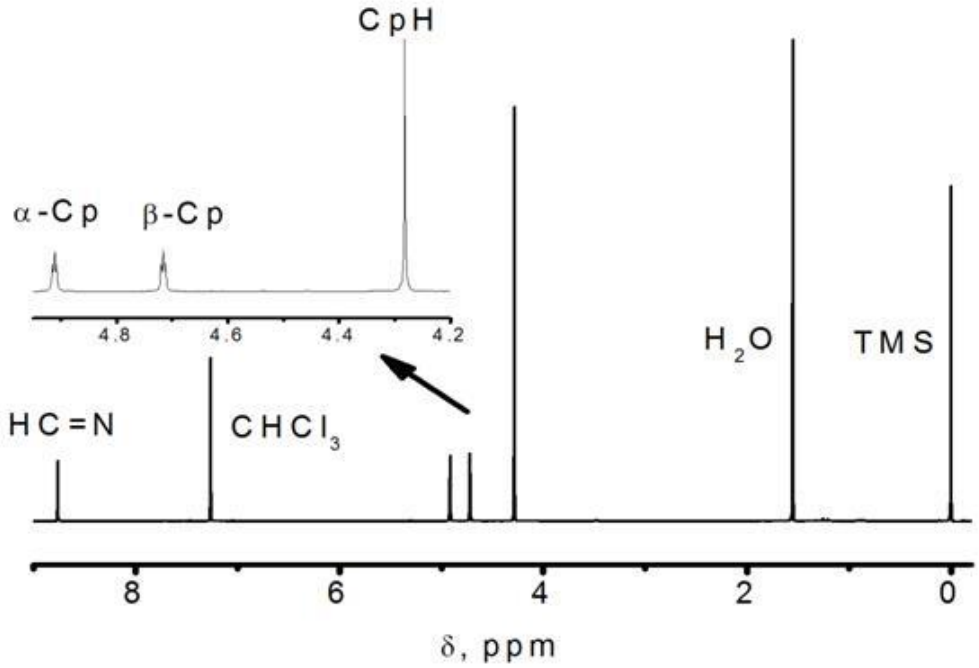

Figure 2. ^{1}H NMR spectrum of **2** in $CDCl_3$.

protons of **1** are present at 4.92 ppm. This peak is slightly broader than the ferrocene peaks due to hydrogen bonding effects. As is the case with carbonyls and their derivatives, the Schiff base proton is farther downfield at 8.37 ppm for **1** and 8.76 ppm for **2**.

The same argument presented for the ^{1}H peak assignments of mono-substituted ferrocene also apply to the ^{13}C spectrum. The carbon attached to the substituent is designated the ipso (*i*) carbon. The two carbons bonded to the *i*-carbon are designated the α-carbons and the remaining two are the β-carbons. The five Cp carbons retain their equivalency and appear as one signal. Compound **1** (Figure 3) has shifts of 69.73 (β-Cp), 70.15 (Cp), 72.93 (α-Cp), and 79.40 (*i*-Cp) ppm. Due to the nuclear Overhauser enhancement (NOE) effect, carbons bonded to more hydrogen atoms generally exhibit a more intense signal in the proton-decoupled carbon spectrum. This effect is clearly evident in the spectra presented here, with the low intensity *i*-Cp carbon having no directly-bonded hydrogens, medium-intensity α-Cp and β-Cp carbons with two hydrogens each, and higher-intensity Cp-H carbons with a total of five hydrogens. Compound **2** (Figure 4) exhibits the same properties with shifts of 70.36 (β-Cp), 70.18 (Cp-H), 73.70 (α-Cp), and 79.08 (*i*-Cp) ppm.

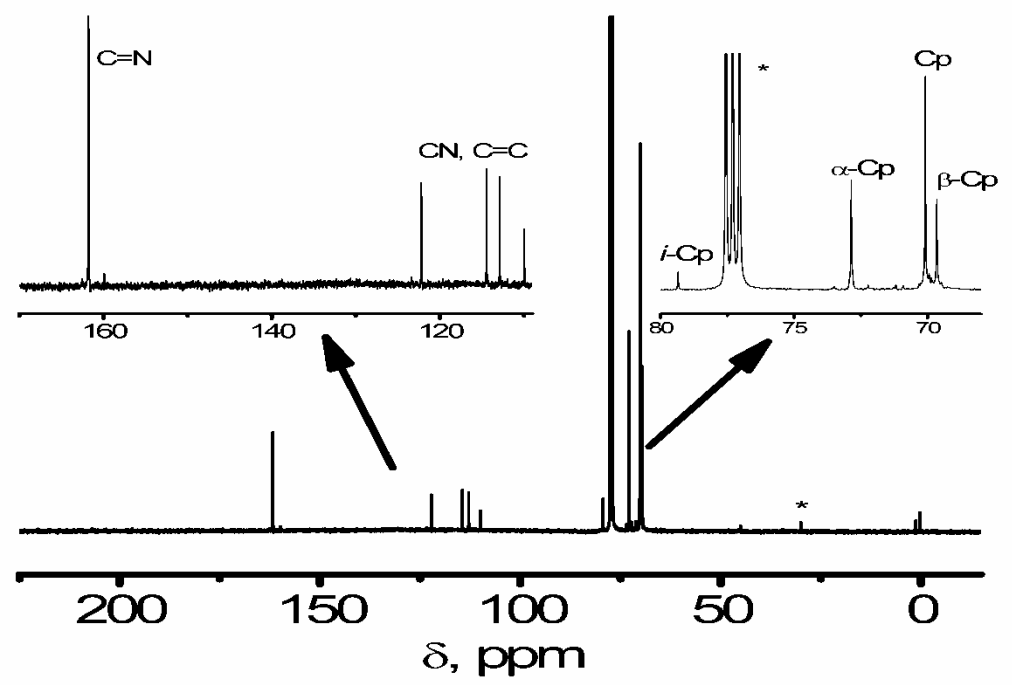

Figure 3. ^{13}C NMR spectrum of **1** in $CDCl_3$.

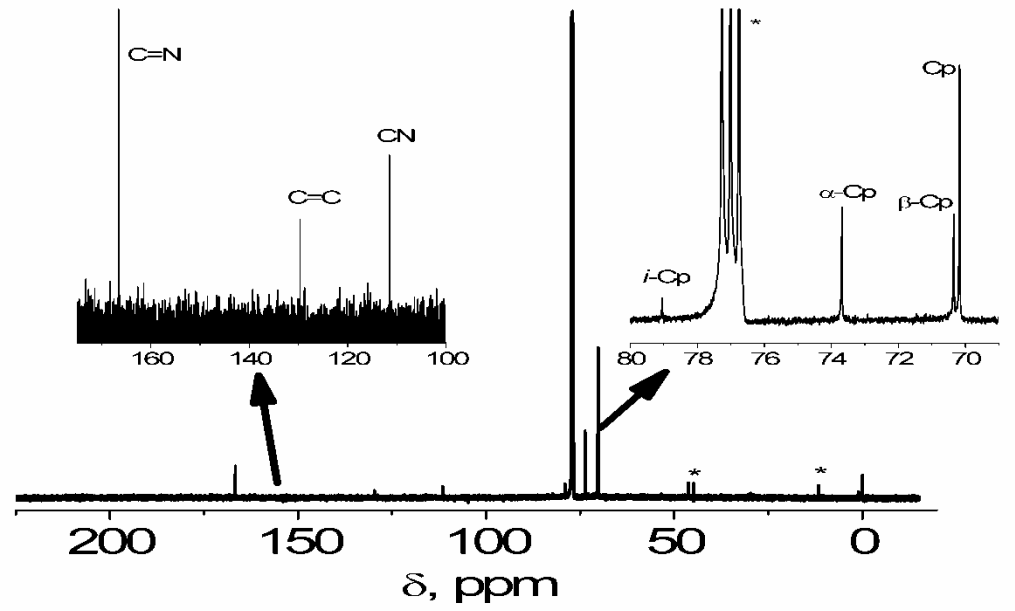

Figure 4. ^{13}C NMR spectrum of **2** in $CDCl_3$.

There are four peaks, at 110.00, 112.94, 114.51, and 122.26 ppm, in the spectrum of **1** that correspond to the two aliphatic double-bonded carbons and the two nitrile carbons. Because these types of carbons typically appear in the same range and in this case have no directly-bonded hydrogens, it is difficult to assign them individually. However, due to the presence of only two peaks in this region, at 111.52 and 129.70 ppm, in the spectrum of the symmetrical compound **2**, it can be concluded that these signals do in fact represent these carbons.

Again, the signals corresponding to the carbonyl-derivative Schiff base are located farthest downfield. A shift of 161.86 ppm appears in the spectrum of **1** and 166.65 ppm in **2**. The remaining peaks, labeled with a star (*), are chloroform, triethylamine, and solvent impurity peaks.

3.3 IR Spectra

The vibrational frequencies are consistent with the functional groups present in **1** and **2**. The primary amine stretch of **1** (Figure 5) appears as the typical doublet with strong absorption frequencies of 3428 and 3320 cm^{-1}. Several weak bands in the area of 3100-3150 cm^{-1} correspond to the ferrocenyl sp^2 C-H stretches. Two medium bands with energies of 2230 and 2199 cm^{-1} correspond to the two different nitrile groups. The separation of these bands is presumably the result of resonance with the conjugated C=C bond, which results in a lower frequency. A strong band at 1602 cm^{-1} is a combination of C=C and C=N stretches, which have similar frequencies. A medium strength shoulder at

1569 cm^{-1} is the N-H bending absorption of the amine. The strong band at 1376 cm^{-1} is the C-N stretch of the amine.

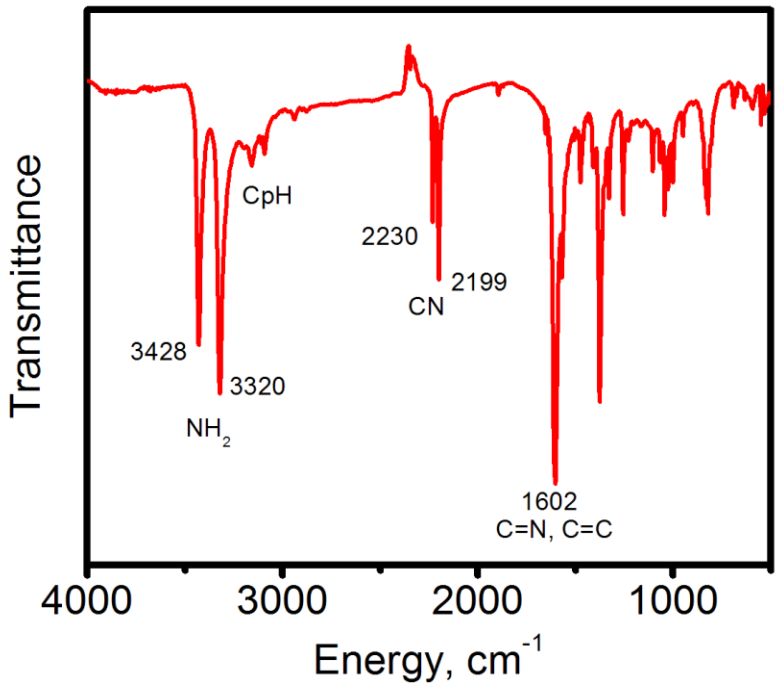

Figure 5. IR spectrum of **1**.

The IR spectrum of **2** (Figure 6) is clearly lacking the primary amine doublet, further confirming the addition of the second Schiff base. Several weak bands around 3000-3100 cm^{-1} are the C-H stretches on ferrocene. A weak, single band at 2212 cm^{-1}, the nitrile stretching frequency, reflects the symmetry of the nitrile groups. A strong band at 1578 cm^{-1} corresponds to the C=N stretch of the Schiff base. This band is at a lower frequency than observed in **1** due to the diminished C=C absorption caused by the symmetry of the vibration, rendering it invisible to IR spectroscopy.

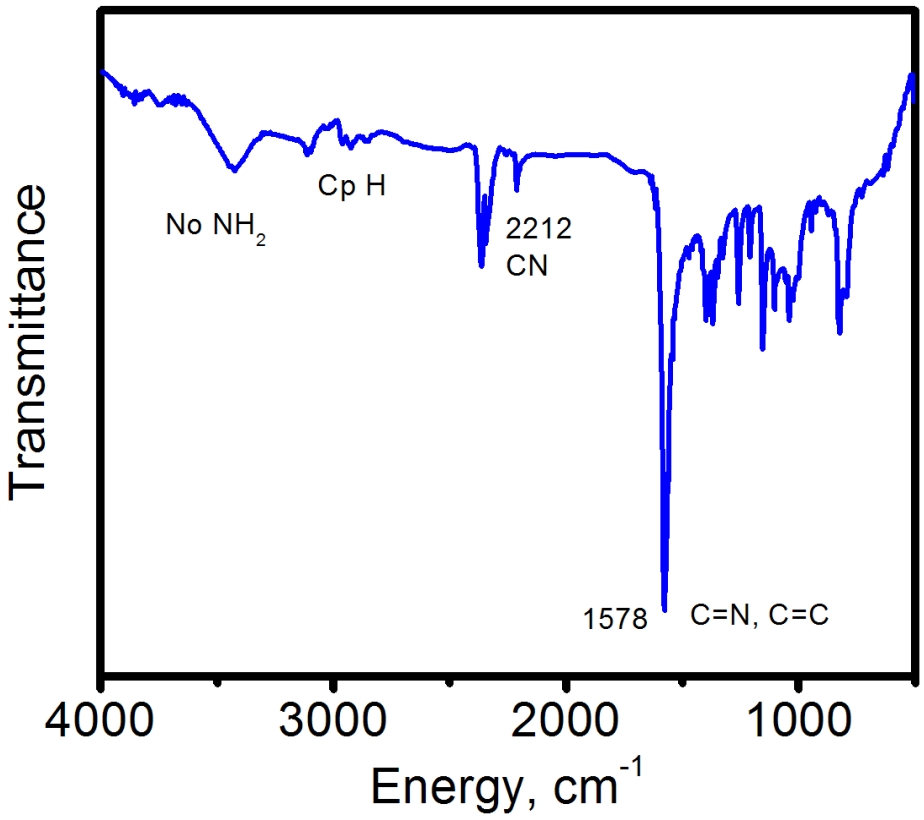

Figure 6. IR spectrum of **2**.

3.4 Crystal Structures

Structures of **1** and **2** exhibit similar yet slightly modified arrangements from their substituent parts. As the crystal structure below reveals, the product **2** has the trans-configuration rather than the initial cis-configuration of DAMN.[45] This isomerization has

been observed in tetramethylated DAMN[46] and is probably due to an increase of steric hindrance that would be present in the cis-isomer. Fe-C distances of the ferrocene unit range from 2.05 – 2.07 Å in **1** (Figure 7) and 2.03 – 2.06 Å in **2** (Figure 8). The Cp rings are slightly tilted, with angles between the averaged distance planes 2.35° in **1** and 2.06° in **2**. The distance between the Cp ring centroids is 3.315 Å in **1** and 3.308 Å in **2**. In comparison, monoclinic ferrocene features a mean Fe-C distance of

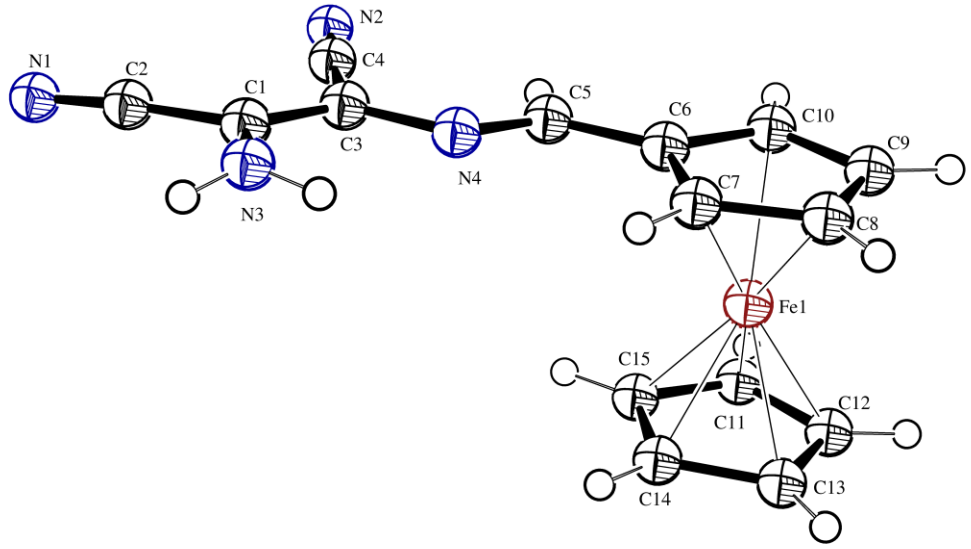

Figure 7. Ortep picture showing crystal structure of **1**, shown with 50% probability ellipsoids.

2.033 Å and a coplanar ring distance of 3.25 Å.[47] These alterations are consistent with other monosubstituted ferrocene products reported in the literature.[48] The Cp rings of ferrocene have been reported to exist in the eclipsed (0°) conformation in the gas phase and staggered (36°) in single crystal structures.[49] Interestingly, the Cp rings of **1** are nearly eclipsed, being offset by 2.28 – 3.49°, while the Cp rings of **2** are nearer to the

staggered conformation with deviations of 23.37 – 26.71°. It has been suggested that such differences are due to intramolecular interactions rather than crystal packing forces.[50]

The Schiff base bond connecting the ferrocene unit to the DAMN backbone is 1.290 Å in **1** (C5-N4) and 1.191 Å in **2** (C7-N8). The remaining amine bond in **1** (C1-N3, 1.35 Å) is shorter than the amine bonds reported in the crystal structure of DAMN (1.398 – 1.387 Å),[51] as are the N-H bonds (0.836, 0.885 Å of **1** vs. 0.87, 0.94, 0.95, 1.02 Å of DAMN). This is a result of the lone pair of electrons on the nitrogen participating in the conjugated π system, thus introducing some double bond character into the C1-N3 bond and pulling the hydrogens closer to help alleviate the loss of electron density. This reduces the acidity of the hydrogens and also shortens the hydrogen bonds from 3.13,

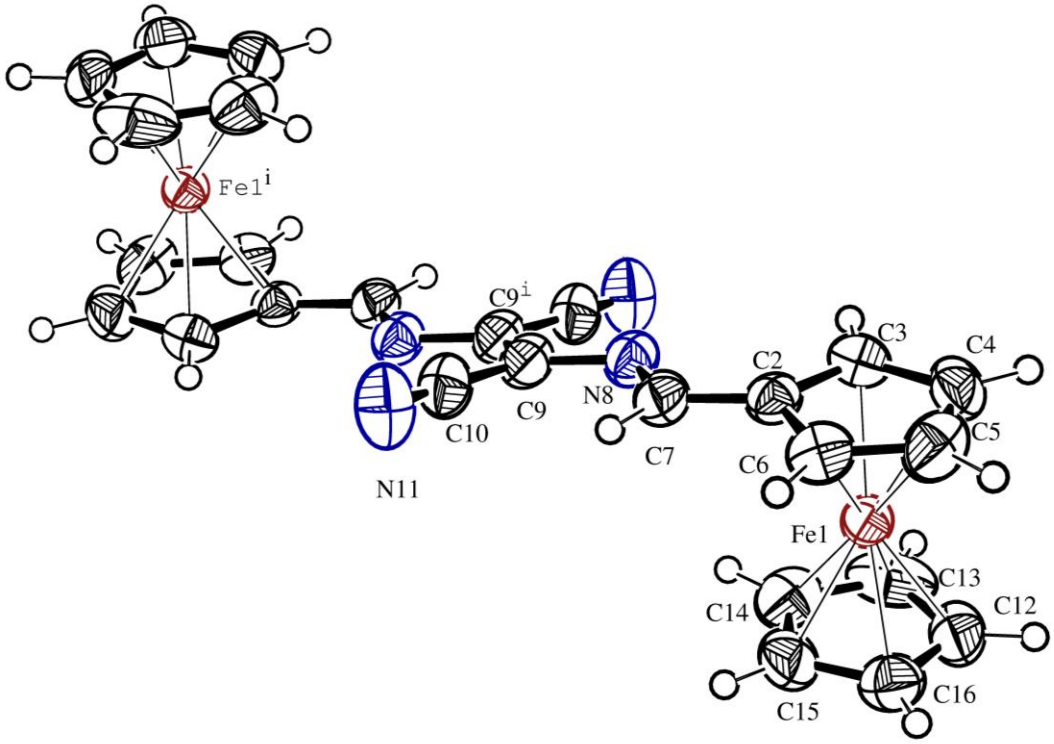

Figure 8. Ortep picture showing crystal structure of **2**, shown with 50% probability ellipsoids.

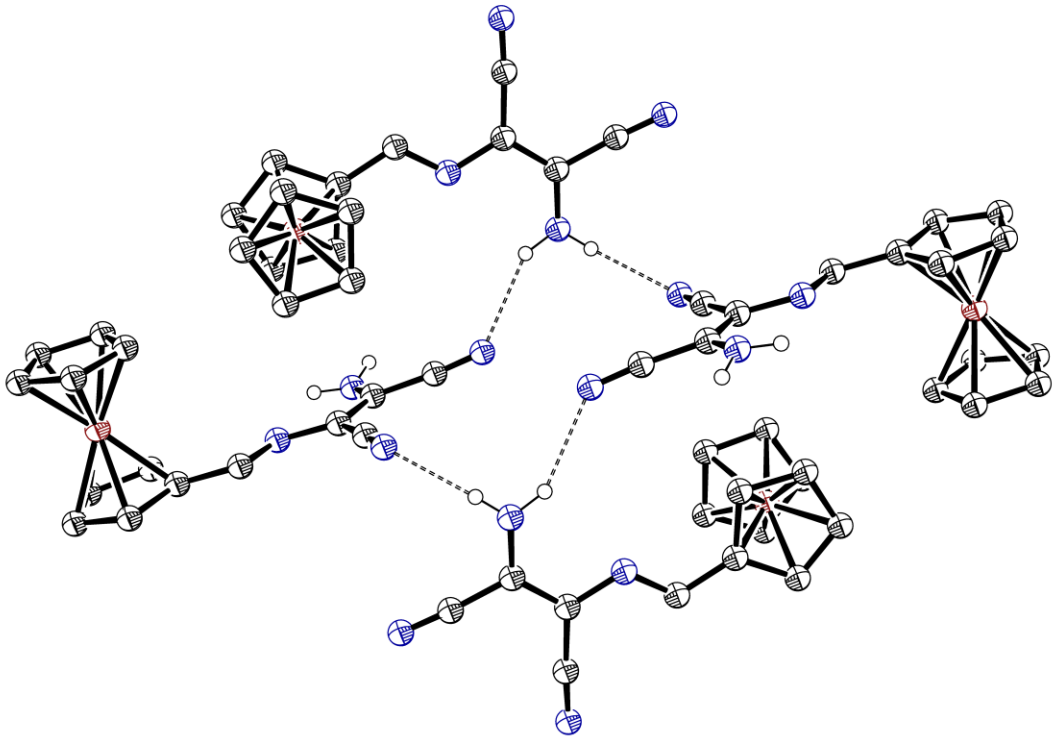

Figure 9. Ortep picture showing hydrogen bonding motif in crystal packing of **1**.

3.22 Å of DAMN. The planar orientation of the amine hydrogens is also a result of the partial double-bond character of the C1-N3 bond. The nitrile bonds have also been contracted, from 1.164, 1.166 Å in DAMN to 1.151 (C17-N18), 1.146 (C19-N20) Å.

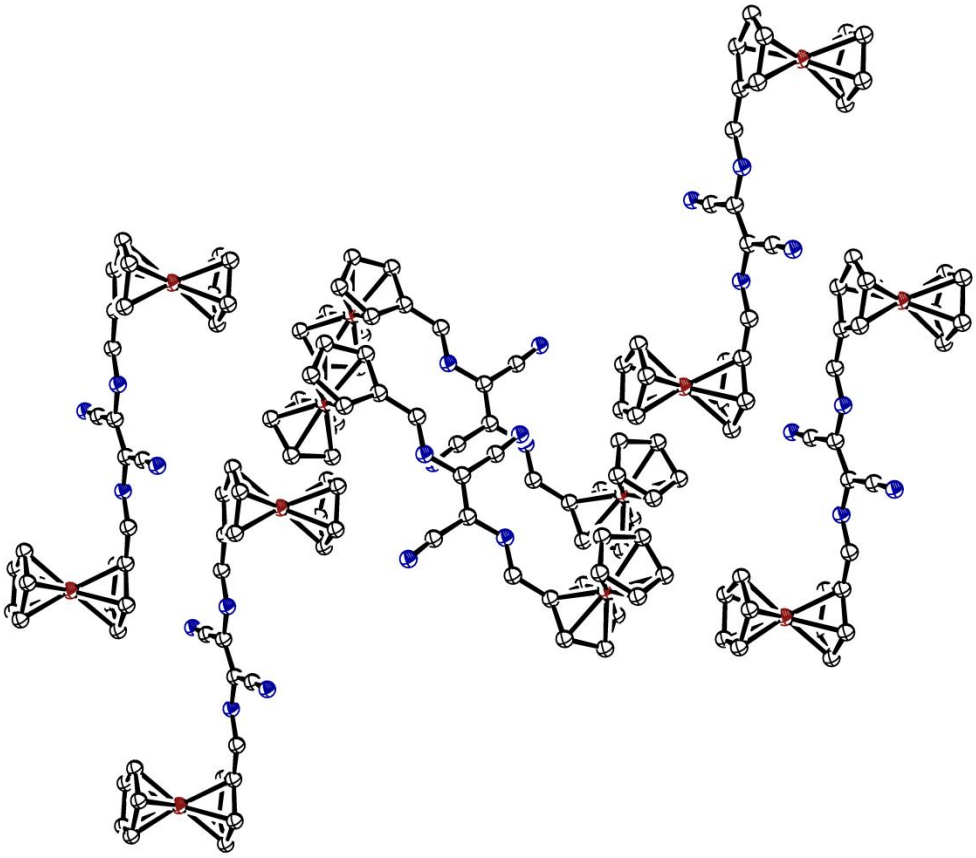

Figure 10. Ortep picture showing crystal packing motif of **2** showing herring-bone arrangement.

Selected crystallographic parameters are summarized in Table 1 below. Both products are crystallized in monoclinic systems with $P2_1/c$ space group and four molecules per cell for **1** and $P2_1/n$ space group with two molecules per cell for **2**. The crystal packing forces of **1** include typical Cp-H interactions of the ferrocene groups as well as the hydrogen bonding of both amine hydrogens (Figure 9), which form hydrogen bonds with differing nitriles of two separate molecules. These hydrogen bonds are relatively weak, with donor ••• acceptor distances of N16 – H ••• N20 = 3.132 Å

(150.50°) and N16 – H ••• N18 = 3.025 Å (166.64°). No hydrogen bonding occurs between molecules of **2**, and therefore interactions between the ferrocene groups dominate its packing structure, and are arranged in a herring-bone fashion (Figure 10).

A comparison of average-distance planes drawn between the carbons of the substituted Cp ring (C6-C10 in **1** and C2-C6 in **2**) and the non-nitrile atoms of the DAMN backbone (C1,C3,N3,N4 in **1**, C9,C9i,N8,N8i in **2**) help illustrate the planarity of the molecules. These planes form angles of 5.93° in **1** and 14.30° in **2**, thus allowing for overlap of the p-orbitals in the conjugated π system.

Table 7. Selected crystallographic parameters of **1** and **2**.

	1	**2**
Empirical Formula	$C_{15}H_{12}N_4Fe$	$C_{26}H_{20}N_4Fe_2$
Formula Weight	304.13	500.17
Crystal System	Monoclinic	Monoclinic
Space Group	$P2_1/c$	$P2_1/n$
Crystal Size (mm^3)	0.20 x 0.10 x 0.05	0.35 x 0.15 x 0.05
Temperature (K)	93	298
***a* (Å)**	10.9199(4)	5.9178(12)
***b* (Å)**	11.1511(3)	21.699(4)
***c* (Å)**	11.7006(8)	8.4626(17)
β (deg)	110.413(8)	95.54(3)
V ($Å^3$)	1335.30(11)	1081.6(4)
Z	4	2
ρ_{calc} (g cm^{-3})	1.513	1.536
μ (mm^{-1})	1.123	1.363
***F*$_{000}$**	624	512
R_1 {$I > 2\sigma(I)$}	0.0286	0.0463
***w*R_2{$I > 2\sigma(I)$}**	0.0670	0.1137
R_1 (all data)	0.0362	0.0828
***w*R_2 (all data)**	0.0710	0.1343
Goodness-of-fit	1.031	1.0052

Table 8. Bond lengths, angles, and dihedral angles of **1**.

1		
N1-C2: 1.146(3)	C2-C1-C3: 119.8(2)	C3-C1-C2-N1: 119.0(2)
N2-C4: 1.151(3)	C3-C1-N3: 124.0(2)	C1-C3-C3-N2: -179.0(3)
C1-N3: 1.346(3)	C1-C3-C4: 121.0(2)	N3-C1-C3-N4: 3.0(3)
C1-C3: 1.373(2)	C1-C3-N4: 117.1(2)	C1-C3-N4-C5: 178.9(2)
C3-N4: 1.396(2)	C3-N4-C5: 121.0(1)	N4-C5-C6-C7: 7.1(3)
N4-C5: 1.290(2)	N4-C5-C6: 119.6(1)	

Table 9. Bond lengths, angles, and dihedral angles of **2**.

2		
N11-C10: 1.134(6)	C10-C9- $C9^{i}$: 118.2(4)	$C9^{i}$-C9-C10-N11: 171(5)
C9-$C9^{i}$: 1.347(7)	$C9^{i}$-C9-N8: 120.0(4)	$C9^{i}$ –C9-N8-C7: 170.3(5)
C9-N8: 1.396(5)	C9-N8-C7: 118.8(4)	N8-C7-C2-C3: 1.7(7)
N8-C7: 1.291(6)	N8-C7-C2: 121.4(4)	

3.5 Electronic Structure

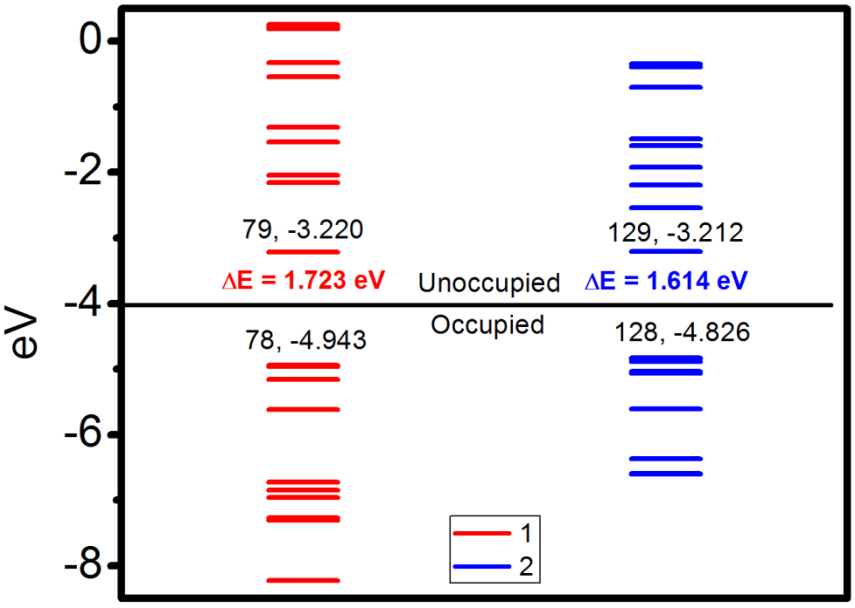

Figure 11. Molecular orbital diagram for **1** and **2**.

Ab-initio DFT calculations were performed to gain insight into the nature of the electronic structure and absorption properties of **1** and **2**. Gas-phase geometries were optimized at the DFT level of theory and confirmed by the positive frequencies of all predicted vibrational modes. The molecular orbital diagram (Figure 11) predicts HOMO-LUMO gap of **2** is smaller than **1** by roughly 100 meV due to the addition of another π-orbital in the conjugated chain. Molecular orbital contributions of individual moieties for **1** and **2** are represented graphically in Figures 12 and 13, respectively. The electronic structures of **1** and **2** feature several parallels. The highest occupied orbitals (HOMO, HOMO-1, HOMO-2, etc.) are predominantly based on the iron centers, and almost entirely based within the ferrocene unit. This is true for the three highest occupied

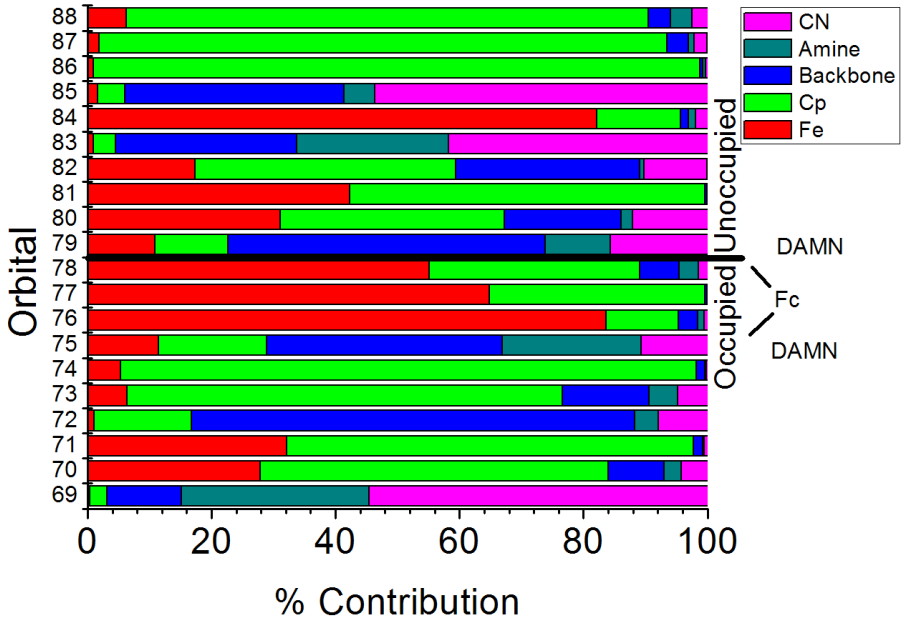

Figure 12. Molecular orbital contributions for **1**.

orbitals (78-76) of **1** and the six highest (128-123) of **2**. These would correspond to the d_z^2, d_{xy}, and $d_{x^2-y^2}$ orbitals of the iron(s). The d_{yz} and d_{xz} antibonding orbitals contribute to orbitals of higher energy. The lowest unoccupied orbital (LUMO) of both molecules (79, 129) is predominantly based on the DAMN unit, as is the orbital below the iron contributors (75, 122). The shift of electron density (Figure 14) between the ferrocene moiety and DAMN backbone from the HOMO to LUMO in both **1** and **2** predicts an intramolecular charge transfer to the excited state.

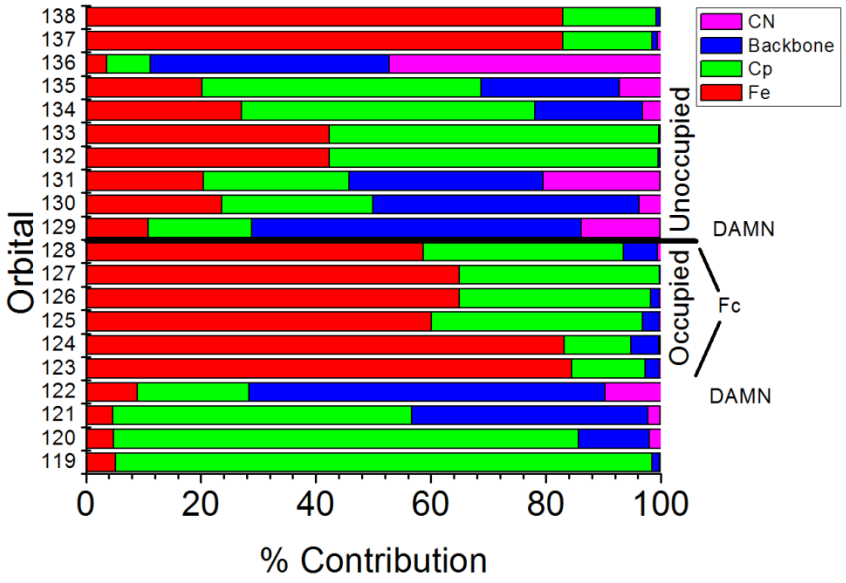

Figure 13. Molecular orbital contributions for **2**.

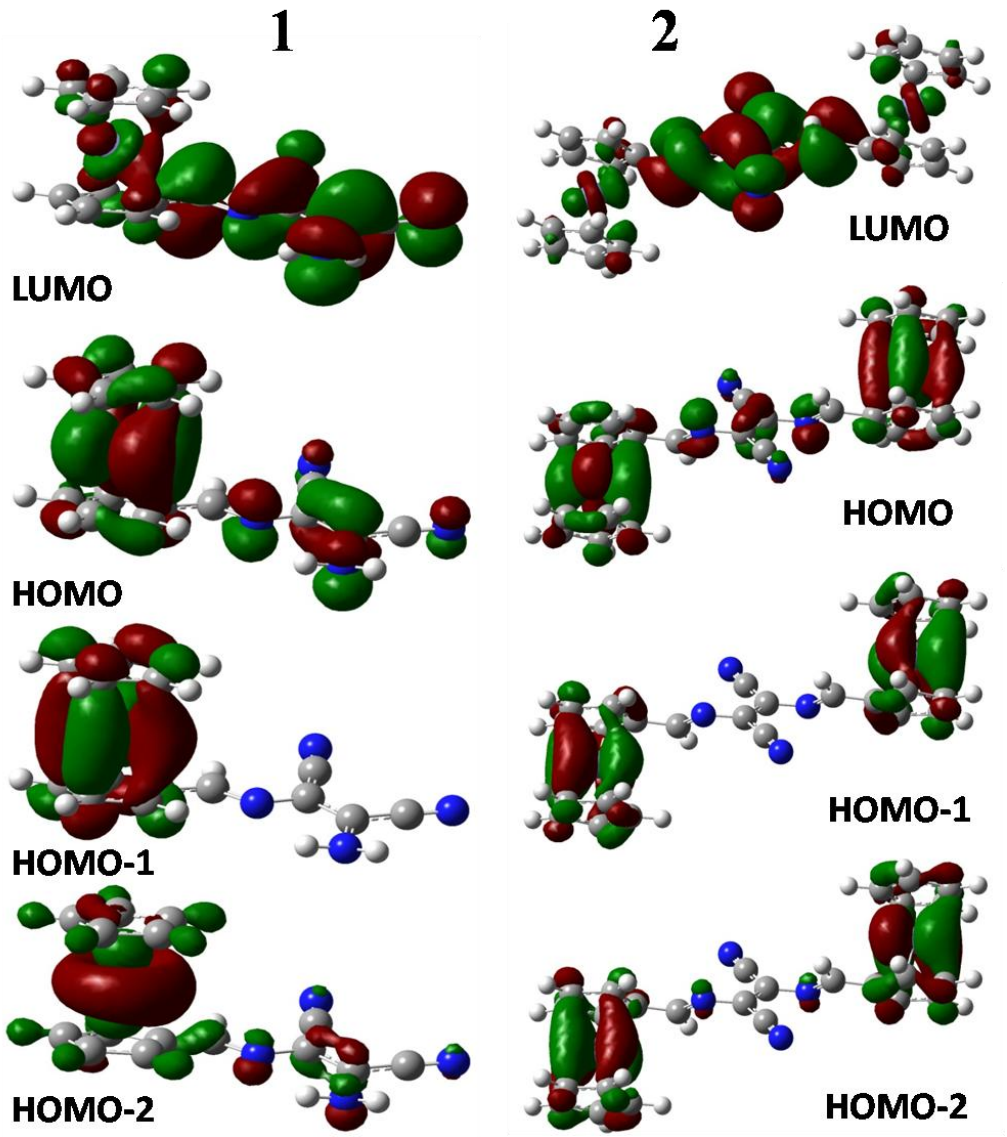

Figure 14. Visual depiction of calculated electron density for selected orbitals of **1** and **2**.

3.6 UV-Vis, TDDFT, and Solvatochromism

Absorption spectra of **1** and **2** in dichloromethane are summarized in Table 4 and shown graphically in Figures 15 and 16, respectively. The spectra of both neutral compounds consist of two main absorptions: a higher-intensity band at 355 nm for **1** and 395 nm for **2** and a lower-intensity band within the visible spectrum which is responsible for the red color of **1** (512 nm) and the blue color of **2** (586 nm). The lower energy spectrum of **2** is consistent with the smaller HOMO-LUMO gap as predicted by the DFT orbital energies.

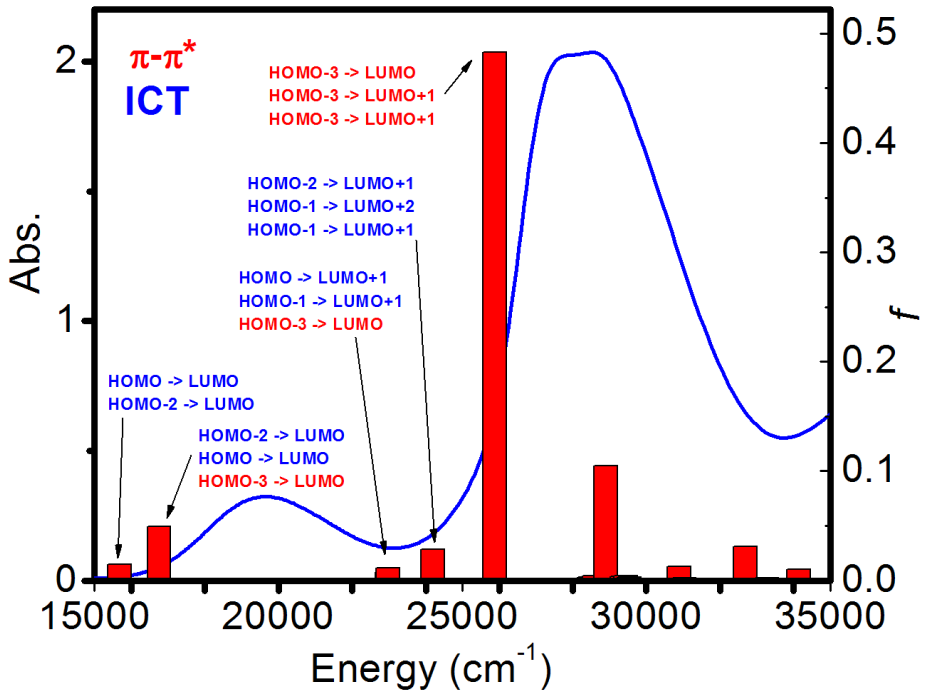

Figure 15. Absorbance spectrum (line) vs. TDDFT excitation energies (bars) for **1**.

Gas phase vertical excitations calculated using the TDDFT approach are listed in Tables 5 and 6 and predict similar, but red-shifted spectra as illustrated in Figures 15 (**1**) and 16 (**2**)**.** Excitations two and three contribute to the low-energy band of **1** and are

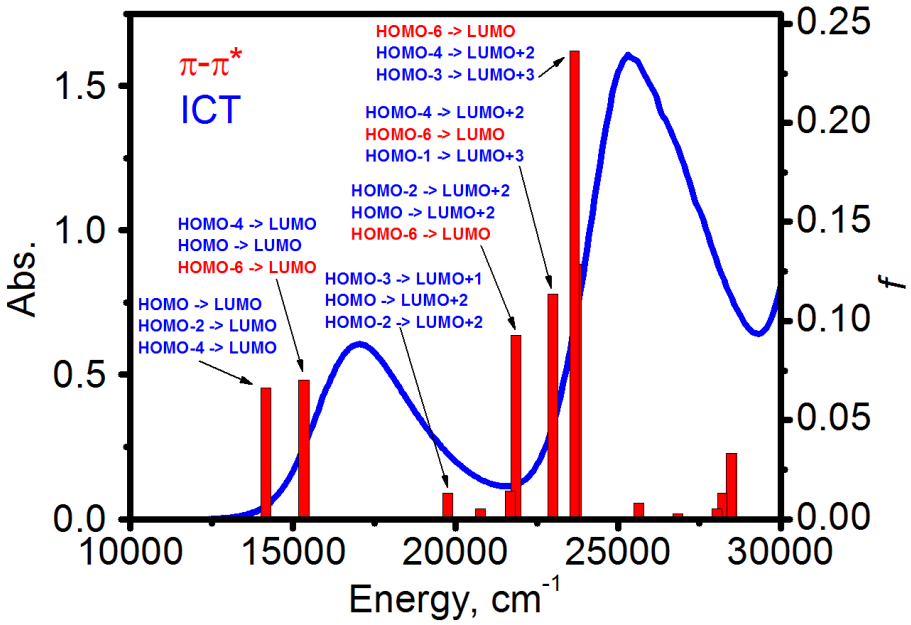

Figure 16. Absorbance spectrum (line) vs. TDDFT excitation energies (bars) for **2**.

comprised mainly of Fc to backbone transitions (100% and 85.7%, respectively). This band can therefore be assigned as an intramolecular charge transfer (ICT) band. Excitation eight, which has the highest oscillator strength near the high-energy band, consists primarily of backbone-based transitions (62.7%) and is therefore assigned as a π-π* band. For **2**, excitations three and five make up the low-energy band. Fc to backbone transitions comprise 83.6% and 95% of this ICT band, respectively. Transition 21, with the highest oscillator strength, correlates to the high-energy band and has as its largest single contributor the π-π* transition (122 -> 129, 30.4%) but consists mainly of a mix of various Fc - Fc and Fc - backbone transitions.

Table 10. Absorption peaks(nm) in DCM and extinction coefficients in parentheses($M^{-1}cm^{-1}$).

	π- π*	**MLCT**	**IVCT**
1	355 (22,500)	512 (3,640)	-
1^+	361 (26,000)	459 (6,240)	-
2	395 (31,600)	586 (11, 900)	-
2^+	403 (17,600)	647 (5,470)	1500 (1,640)
2^{2+}	366 (11,300)	633 (1,770)	-

Absorption properties were further investigated by recording spectra in solvents of various polarities to elucidate any solvatochromic effect. Indeed, a significant difference of 41 nm (1721 cm^{-1}, 0.213 eV) was observed in the ICT band of **1** (Figure 17) and a difference of 27 nm (816 cm^{-1}, 0.101 eV) in the ICT band of **2** (Figure 18), while the π - π* band remained largely unaffected. An attempt was made to correlate the shift

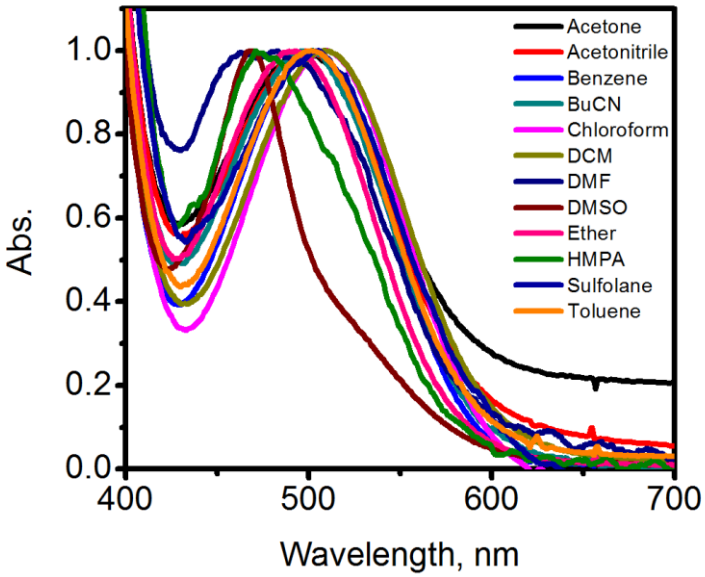

Figure 17. Normalized absorption spectra of **1** showing solvatochromic shift of ICT band.

with empirical solvent parameters α, β, and π* of the Kamlet-Taft model.[52] These parameters give a measure of the solvent's hydrogen bond donating capability, hydrogen

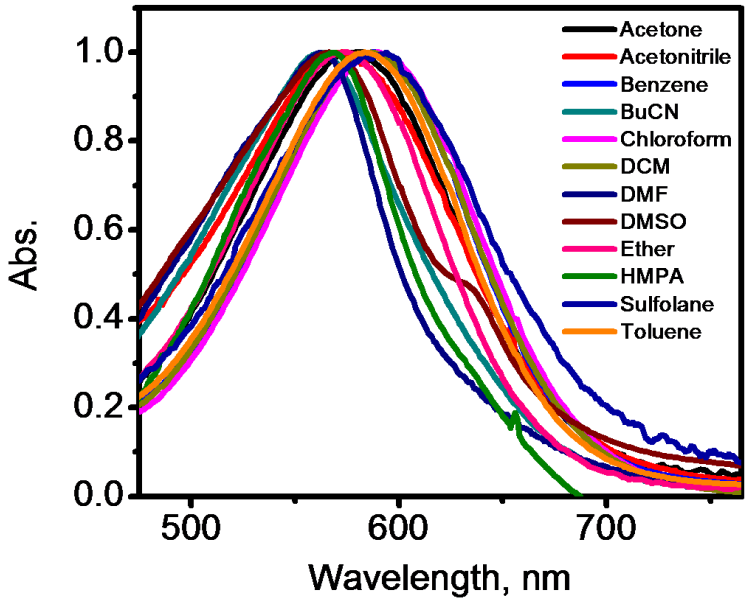

Figure 18. Normalized absorption spectra of **2** showing solvatochromic shift of ICT band.

bond accepting capability, and polarizability, respectively. Only minimal correlations were observed between the observed MLCT band energy and these parameters, suggesting a more complex relationship within the solvation sphere of the compounds.

Table 11. TDDFT excitation energies of **1**. HOMO and LUMO orbitals are in bold.[a]

State	Wave-length (nm)	Energy (eV)	*Oscill. Strength (f)*	Expansion Coefficients			
1	695.78	1.7819	0.0002	77 -> **79**	0.68461	**78** -> **79**	-0.12359
2	637.64	1.9444	0.0147	76 -> **79**	0.47313	**78** -> **79**	0.47081
3	596.83	2.0774	0.0490	75 -> **79**	0.25225	76 -> **79**	0.48814
				78 -> **79**	-0.38081		
4	435.81	2.8449	0.0080	77 -> 80	0.42629	77 -> 81	0.21646

				78 -> 80	-0.41002	**78** -> 81	0.28363
5	435.20	2.8489	0.0118	75 -> **79**	0.10212	77 -> 80	0.40634
				77 -> 81	-0.26577	**78** -> 80	0.41555
				78 -> 81	0.25351		
6	413.24	3.0003	0.0286	75 -> **79**	-0.13699	76 -> 80	0.61391
				77 -> 81	-0.28470		
7	404.90	3.0621	0.0002	76 -> 81	0.49631	77 -> 80	-0.19316
				77 -> 81	0.15761	77 -> 82	-0.10308
				78 -> 81	0.40152		
8	386.50	3.2079	0.4831	75 -> **79**	0.47625	75 -> 80	0.29411
				76 -> 80	0.17488	**78** -> **79**	0.13233
9	374.69	3.3090	0.0007	75 -> 81	-0.15562	76 -> 81	0.37952
				77 -> 80	0.18354	77 -> 82	0.44000
				78 -> 81	-0.26230		
10	371.64	3.3362	0.0012	76 -> 80	0.19519	76 -> 81	-0.14427
				76 -> 82	0.18637	77 -> 81	0.37319
				78 -> 80	0.23036	**78** -> 82	0.39416
11	351.39	3.5284	0.0030	74 -> **79**	0.63314	75 -> 80	0.14585
				75 -> 81	0.17026	77 -> 82	0.16163
				78 -> 82	-0.10179		
12	349.86	3.5438	0.0045	74 -> **79**	-0.27438	75 -> 81	0.49540
				76 -> 81	-0.11226	77 -> 82	0.34058
13	346.04	3.5829	0.1049	73 -> **79**	-0.17286	74 -> **79**	-0.10086
				75 -> **79**	-0.12934	75 -> 80	0.32581
				75 -> 81	-0.14160	76 -> 82	0.35630
				77 -> 82	-0.14930	**78** -> 82	-0.32113
14	340.82	3.6378	0.0035	**78** -> 83	0.70166		
15	339.74	3.6493	0.0044	77 -> 83	0.70434		
16	338.69	3.6607	0.0030	73 -> **79**	0.49184	75 -> 80	-0.28418
				76 -> 82	0.31945	**78** -> 82	-0.20396
17	327.46	3.7862	0.0012	72 -> **79**	0.63337	73 -> **79**	0.18619
				76 -> 82	-0.17106		
18	323.74	3.8298	0.0131	70 -> **79**	-0.14828	72 -> **79**	0.24145
				73 -> **79**	-0.13848	75 -> 82	0.11921
				76 -> 80	-0.10881	76 -> 82	0.40455
				77 -> 81	-0.20707	**78** -> 80	-0.14835
				78 -> 82	0.25088		
19	322.44	3.8452	0.0009	71 -> **79**	0.17364	75 -> 81	-0.32530
				76 -> 81	-0.17236	76 -> 83	0.39188
				77 -> 80	-0.14003	77 -> 82	0.25657
				78 -> 81	0.18802		
20	322.28	3.8471	0.0022	71 -> **79**	-0.11919	75 -> 81	0.21109
				76 -> 81	0.11762	76 -> 83	0.58568
				77 -> 82	-0.16266	**78** -> 81	-0.12024
21	305.91	4.0530	0.0308	70 -> **79**	0.36342	71 -> **79**	-0.15552
				72 -> **79**	-0.11773	73 -> **79**	0.25772
				74 -> 81	-0.10958	75 -> **79**	-0.10063
				75 -> 80	0.23863	75 -> 82	-0.17017
				77 -> 81	-0.12951	**78** -> 82	0.21158

22	300.58	4.1249	0.0022	70 -> **79**	0.18333	71 -> **79**	0.63258
23	292.90	4.2329	0.0104	70 -> **79**	0.41002	70 -> 80	-0.11579
				75 -> 82	0.50492		
24	285.66	4.3403	0.0013	75 -> 83	0.69393		
25	281.88	4.3985	0.0001	**78** -> 84	0.70653		
26	280.77	4.4159	0.0000	77 -> 84	0.70683		
27	270.52	4.5831	0.0024	73 -> 81	-0.10878	74 -> 80	0.67670
28	268.66	4.6150	0.0043	74 -> 80	0.10368	76 -> 84	0.65732
				77 -> 85	-0.12338	**78** -> 85	0.17124
29	268.25	4.6220	0.0000	76 -> 84	-0.19408	**78** -> 85	0.67534
30	267.60	4.6331	0.0008	76 -> 84	0.12432	77 -> 85	0.67684
				78 -> 85	0.10687		

[a] All transitions have A symmetry.

Table 12. TDDFT excitation energies of **2**. HOMO and LUMO orbitals are in bold.

State	**Symm.**	**W (nm)**	**E (eV)**	***Osc. Str. (f)***	**Expansion Coefficients**			
1	A_g	749.62	1.6540	0.0000	127 ->**129**	0.70089		
2	A_u	749.59	1.6540	0.0007	**126 ->129**	0.60411	**128 ->129**	0.35474
3	A_u	706.00	1.7562	0.0656	124 ->**129**	0.25589	125 ->130	-0.10301
					126 ->**129**	0.32314	**128** ->**129**	0.53227
4	A_g	699.87	1.7715	0.0000	123 ->**129**	-0.18065	125 ->**129**	0.65479
					128 ->130	-0.11199		
5	A_u	652.16	1.9011	0.0700	122 ->**129**	0.14114	124 ->**129**	0.64012
					128 ->**129**	-0.18924		
6	A_g	644.02	1.9252	0.0000	123 ->**129**	0.66650	125 ->**129**	0.14727
7	A_g	527.27	2.3514	0.0000	126 ->130	0.56582	127 ->131	0.10445
					128 ->130	-0.38758		
8	A_u	527.20	2.3518	0.0007	127 ->130	0.68528		
9	A_g	506.22	2.4492	0.0000	124 ->130	0.12188	125 ->131	-0.19480
					126 ->130	0.35530	**128** ->130	0.50786
10	A_u	506.01	2.4503	0.0129	125 ->130	0.64528	126 ->131	-0.12498
					128 ->131	-0.17960		
11	A_g	484.99	2.5564	0.0000	124 ->130	0.67579		
12	A_u	481.48	2.5751	0.0053	123 ->130	0.69267		
13	A_u	461.21	2.6883	0.0140	126 ->131	0.43728	**128** ->131	-0.50172
14	A_g	460.6	2.6917	0.00	127 ->131	0.67052	**128** ->132	-0.13819

		2		00				
15	A_u	457.47	2.7102	0.0895	122 ->**129**	0.19004	125 ->130	0.13766
					126 ->131	0.48261	127 ->132	0.14566
					128 ->131	0.36709	**128** ->133	-0.11806
16	A_g	448.65	2.7635	0.0000	125 ->131	0.63051	126 ->132	-0.16800
					127 ->133	-0.18886		
17	A_u	434.86	2.8511	0.1106	122 ->**129**	-0.26883	124 ->131	0.58926
					126 ->133	0.11016	127 ->132	0.13981
18	A_g	427.91	2.8974	0.0000	123 ->131	0.69461		
19	A_u	425.27	2.9154	0.0006	126 ->133	-0.36111	127 ->132	0.49208
					128 ->133	0.34734		
20	A_g	425.14	2.9163	0.0000	126 ->132	-0.39906	127 ->133	0.49592
					128 ->132	0.29915		
21	A_u	422.63	2.9336	0.2206	118 ->**129**	0.10690	122 ->**129**	0.36704
					122 ->131	0.17521	124 ->131	0.27314
					125 ->132	0.26500	126 ->133	0.23373
					128 ->131	-0.10921	**128** ->133	0.23472
22	A_g	422.24	2.9363	0.0000	125 ->133	0.42931	126 ->132	0.31620
					128 ->132	0.44472		
23	A_u	421.77	2.9396	0.1358	122 ->**129**	-0.29008	122 ->131	-0.14455
					124 ->131	-0.19143	125 ->132	0.34235
					126 ->133	0.27879	**128** ->133	0.32808
24	A_u	406.51	3.0499	0.0001	123 ->132	-0.27958	124 ->133	-0.22375
					125 ->132	0.47601	126 ->133	-0.20197
					127 ->134	-0.15831	**128** ->133	-0.23876
25	A_g	406.39	3.0509	0.0000	123 ->133	-0.27507	124 ->132	-0.22918
					125 ->133	0.47781	126 ->132	-0.19266
					126 ->134	-0.12843	**128** ->132	-0.23860
26	A_g	396.83	3.1244	0.0000	123 ->133	-0.38910	124 ->132	0.58648
27	A_u	396.79	3.1247	0.0000	123 ->132	-0.38839	124 ->133	0.58237
28	A_g	391.58	3.1663	0.0000	122 ->130	0.19125	124 ->134	0.10792
					125 ->131	-0.12986	126 ->132	-0.25495
					126 ->134	0.23424	127 ->133	-0.30357
					128 ->132	0.16443	**128** ->134	0.38131
29	A_g	390.02	3.1790	0.0000	121 ->**129**	-0.38747	122 ->130	0.54349
30	A_u	389.71	3.1815	0.0077	123 ->134	-0.11968	125 ->134	0.37066
					126 ->133	0.27583	127 ->132	0.34116
					127 ->134	-0.11821	**128** ->133	-0.20298

3.7 Electro- and Spectroelectrochemistry

Electrochemical experiments were performed in order to understand the influence of oxidation state in **1** and **2** on their absorption spectra. With an understanding of the band assignments, changes in the absorption spectra upon oxidation reveal further insight into electronic structure. Particularly, the appearance of a charge transfer band upon oxidation of **2** to $\mathbf{2}^{+}$ is evident of a mixed-valence species, which is a common phenomena in linked-ferrocenyl compounds.

As expected, one reversible oxidation process was observed in cyclic and differential pulse voltammetry of **1** (Figure 19). The couple exhibits a $E°_{1/2}$ of 0.134 V in 0.10 M TBAP acetonitrile system compared to the ferrocene/ferrocenium redox couple. This anodic shift is in agreement with the presence of a strong electron-withdrawing substituent. Upon oxidation, the absorption spectrum of **1** reveals a significant blue shift

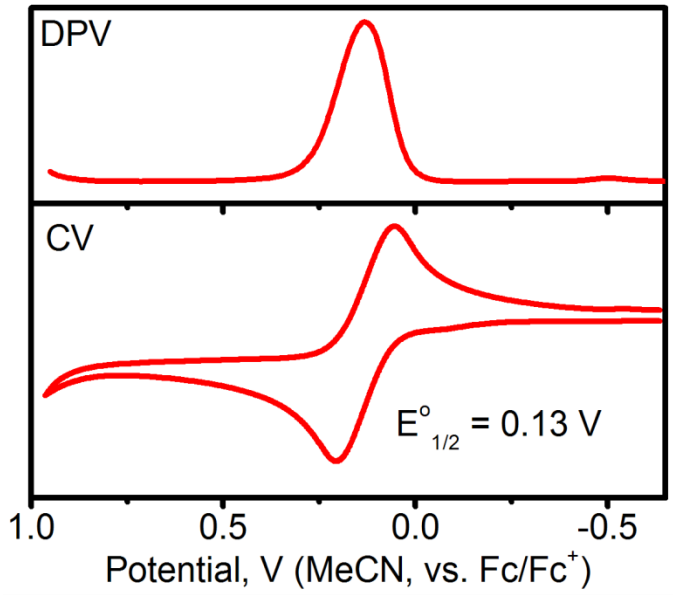

Figure 19. Differential pulse and cyclic voltammetry of **1** in 0.10 M TBAP/acetonitrile system.

of the ICT band from 543 nm to 451 nm, while the π - π* band remains largely unchanged (Figure 20). This means that upon oxidation more energy is required to transfer electron density from the ferrocene to the backbone, suggesting that the electron is in fact removed from the iron center.

Chemical oxidation of **1** was performed by adding silver triflate to a DCM solution. The results are discussed in the cation sensing section below.

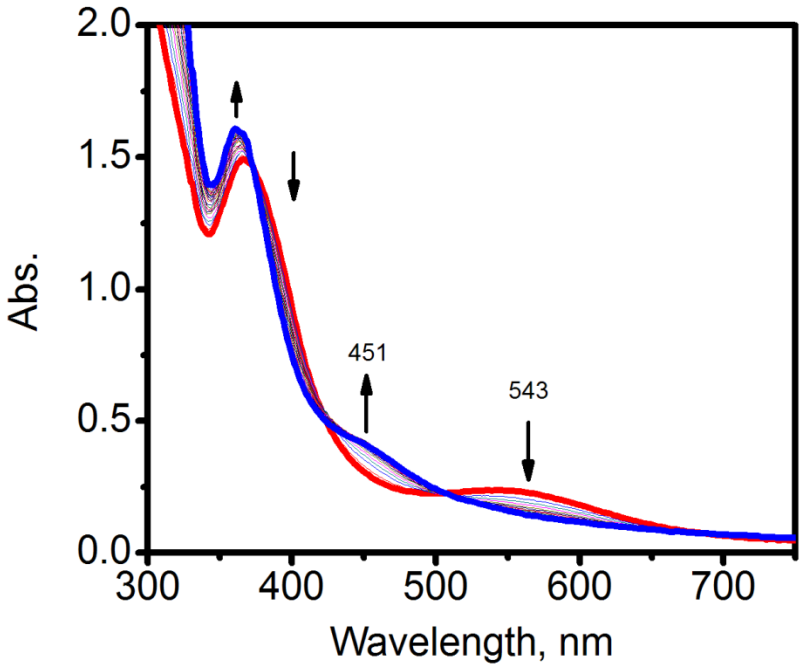

Figure 20. Controlled potential electrolysis of **1** in 0.05M TFAB/DCM system.

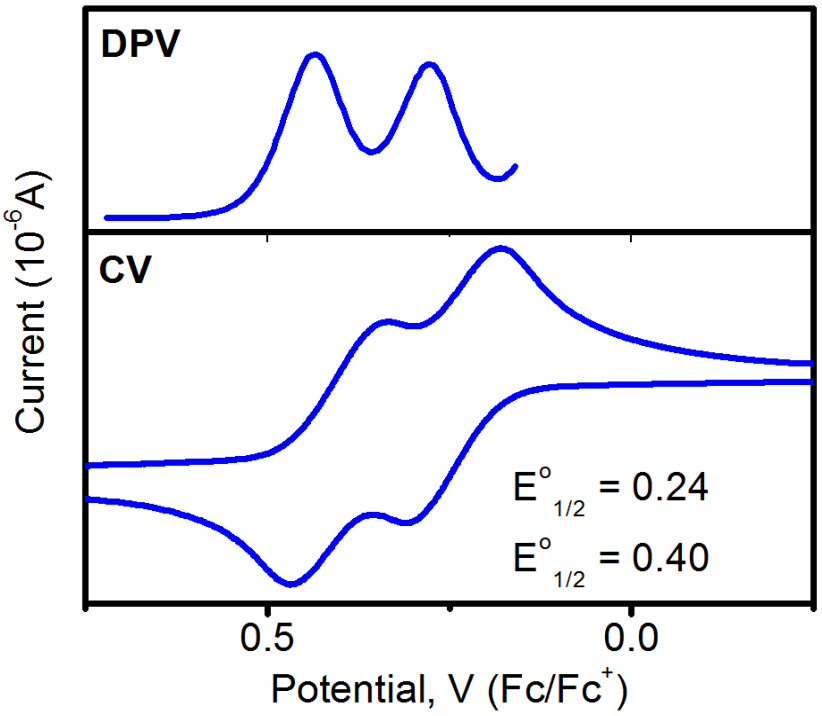

Figure 21. Differential pulse and cyclic voltammetry of **2** in 0.05M TFAB/DCM system.

Two reversible processes were observed in voltammetry of **2** in 0.05 M TFAB DCM system (Figure 21). These were observed at $E°_{1/2}$ values of 0.40 V and 0.24 V, a difference of 160 mV. This separation suggests that removal of an electron from one iron center stabilizes the other iron center, and thus more energy is required to remove a second electron. This is a result of communication between these centers. Indeed,

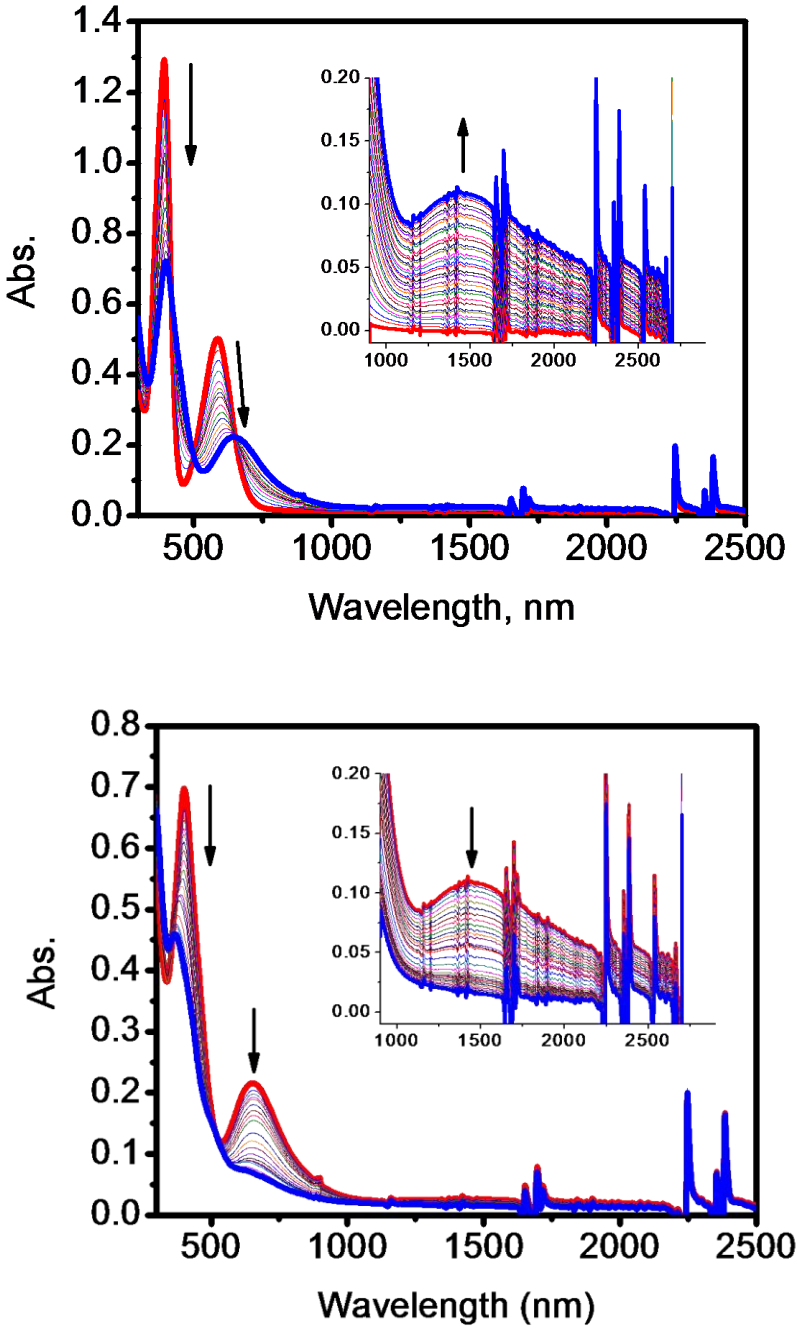

Figure 22. Step-wise oxidation of **2** into $\mathbf{2}^{+}$ (top) and $\mathbf{2}^{2+}$ (bottom) under controlled potential electrolysis in 0.15M TFAB/DCM system. Insets correspond to IVCT band in experiments with 3x concentration.

changes in the UV spectrum upon oxidation confirm the formation of mixed-valence properties in $\mathbf{2}^{+}$. A decrease in intensity of both bands of the neutral **2** indicates a decrease in excitations originating from the ferrocene unit, particularly the iron centers. Meanwhile, the formation of an IVCT band in the near-infrared region (Figure 22) confirms a thermal energy barrier present in $\mathbf{2}^{+}$ allowing for the promotion of an electron to the excited state and relaxation to either center. Further oxidation to $\mathbf{2}^{2+}$ reveals the disappearance of the IVCT band and further loss of intensity in the other bands (Figure 22), confirming the presence of mixed-valence properties of the singly-oxidized species.

Gaussian fitting of the IVCT band in $\mathbf{2}^{+}$ gave the necessary information for calculation of H_{ab} and α via equations (1) and (2). The maximum molar absorption coefficient of 1637 cm^{-1}, energy of ν_{max} of 1462 nm (6840 cm^{-1}), half peak width of 670 cm^{-1}, and distance between centers of 10.75 Å yielded H_{ab}= 166 cm^{-1} and α = 0.0243. These data clearly suggest that $\mathbf{2}^{+}$ belongs to a weakly-coupled class II mixed-valence system.

Chemical oxidation of **2** by silver triflate was performed in DCM solution (Figure 23). The change observed in the absorption spectrum is consistent with the change observed for the first electrochemical oxidation, *i.e.* decrease of intensity of both absorption bands. The IVCT band was observed as a very broad band, making analysis by the Hush method impractical. This could be due to interference caused by free ions in solution.

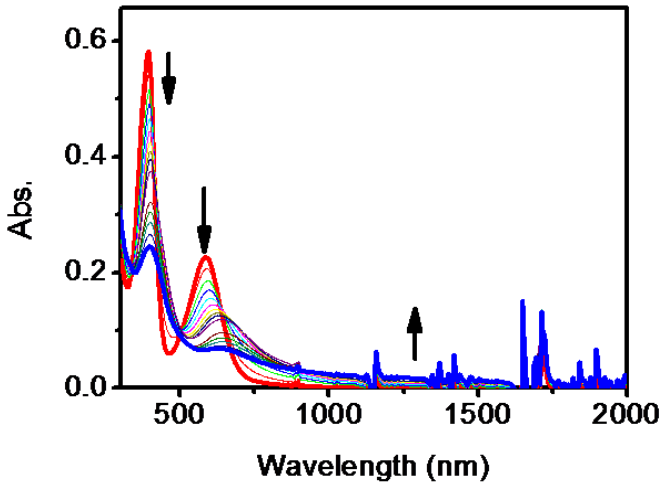

Figure 23. Change in UV spectrum of **2** upon oxidation by silver triflate in dichloromethane.

3.8 Cation Recognition Study

The electron-rich π system of the backbone provides a potential binding site for electron-deficient species such as cations. Analysis of the UV spectrum of **1** and **2** has shown that the absorption bands contain large contributions from transitions to/from orbitals that comprise the backbone, and any perturbation of these orbitals should be reflected in the absorption spectrum. Furthermore, such perturbations could also be reflected electrochemically, as the backbone has been shown to anodically shift the redox potential of the ferrocene moiety. A fluctuation of the electron-withdrawing capability of the backbone should be reflected by a change in the redox potential.

Initial screening of the chemosensing capabilities of **1** and **2** was performed by monitoring the absorption spectrum in the presence of the environmentally-relevant cations Ag^{+}, Ca^{2+}, Cu^{2+}, Hg^{2+}, K^{+}, Li^{+}, Mg^{2+}, Na^{+}, Ni^{2+}, Pb^{2+}, Zn^{2+}, and Cd^{2+}. An excess

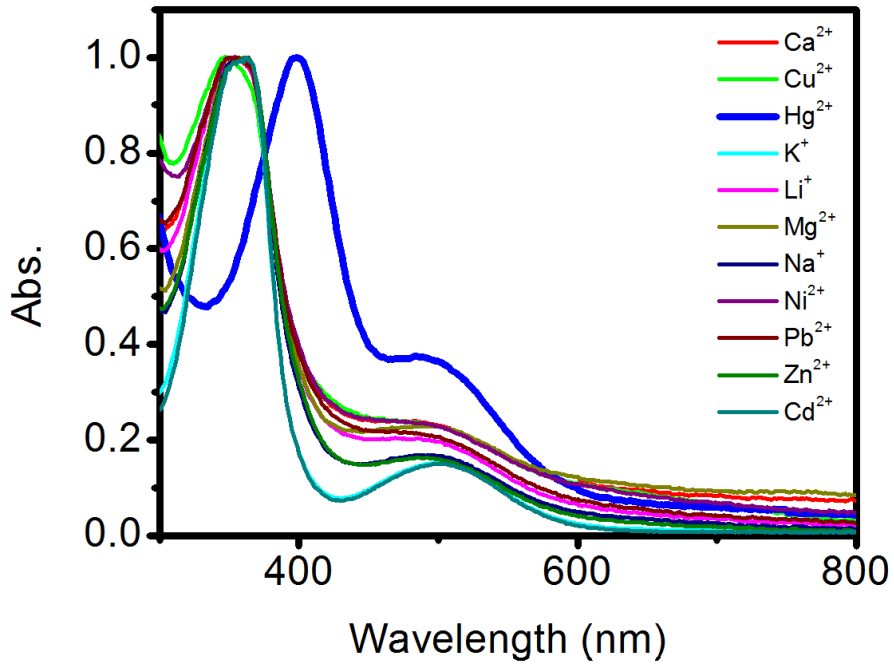

Figure 24. Normalized absorption spectra of **1** in the presence of various cations.

(10 eq.) of the respective metal salt was added to solutions of **1** in acetonitrile and **2** in tetrahydrofuran. In all cases, the addition of the metal salt yielded negligible change in the absorption spectrum of **1** except for the presence of Hg^{2+} and Ag^{+} ions, which produced a shift of the main absorption peak (Figure 24). To test this selectivity and potential interference from the other test cations, absorption spectra of **1** were recorded in acetonitrile in the presence of no cations, all cations except Hg^{2+}, and all cations

including Hg^{2+}. The result shows that ligand **1** selectively binds to Hg^{2+} even in the presence of these other cations. In addition, it was found that the presence of water shows no hindrance to the ability of **1** to bind to Hg^{2+}. The possible modes of interaction between **1** with Hg^{2+} and Ag^{+} are discussed below.

No shifts were observed in the spectrum of **2** upon addition of the metal salts, except for Ag^{+}, which was discussed above. Hence, its chemosensing properties were investigated no further.

Hg^{2+} Recognition. Increasing the concentration of Hg^{2+} resulted in a red-shift of the π - π* band from 362 nm to 393 nm (Δ = 31nm, Figure 25), resulting in a visible color change from red to orange. The process reached the end point after the addition of one

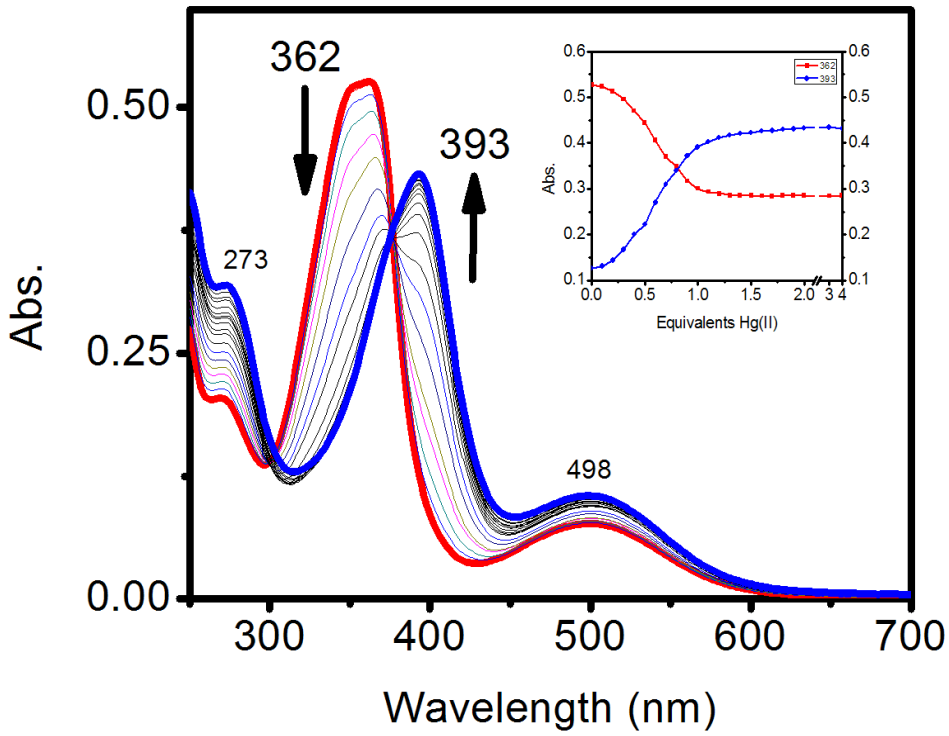

Figure 25. Evolution of absorption spectrum of **1** in acetonitrile upon increasing concentration of Hg^{2+}.

molar equivalent of Hg^{2+}. No change was observed in the energy of the ICT band, implying that the π orbitals of the backbone play a key role in the interaction between the ligand and mercury ion. In comparing this result to the oxidation profile of **1** it can be deduced that the interaction is a result of a complexation process rather than a reduction-oxidation process, as there was no shift in the ICT band. A well-defined isosbestic point at 377 nm signifies an interconversion from the neutral ligand **1** to the complexation product. A similar transition took place upon addition of Hg^{2+} to **1** in ethanol solution (365 to 395 nm, Δ = 30 nm), implying that solvent molecules play a small, if any, role in the complexation process.

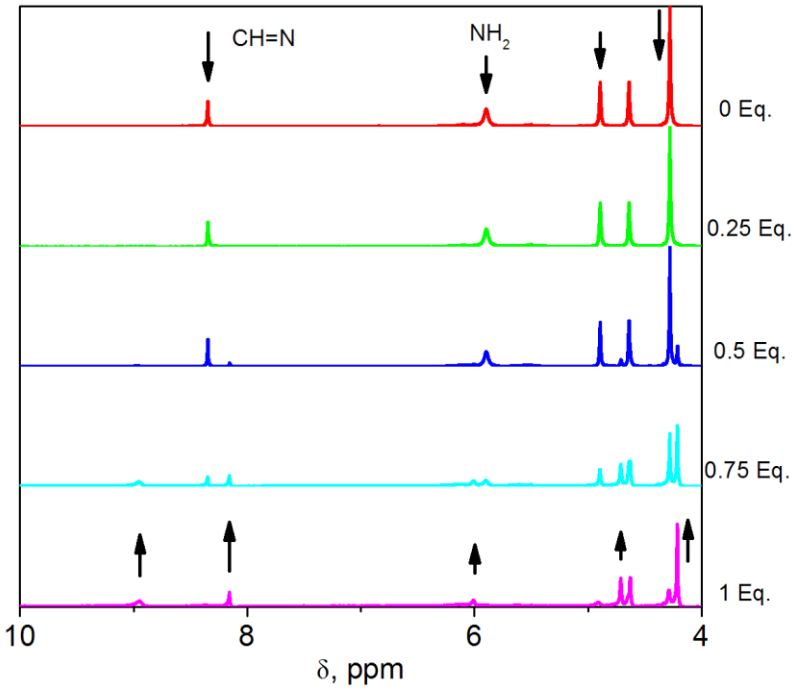

Figure 26. Partial NMR spectra of **1** in CD_3CN, showing evolution of peaks with gradual increase in concentration of Hg^{2+}.

NMR analysis was performed to aid understanding the exact location of mercury coordination. Slowly increasing the concentration of Hg^{2+} leads to a shift of nearly all protons in the ^{1}H spectrum, noticeably the Schiff base and amine signals (Figure 26). Fast addition of an excess of Hg^{2+} resulted in a splitting of the amine peak and broadening of the amine, Schiff base, and ferrocene signals (Figure 27). Splitting of the amine peak implies that one of the hydrogens lies closer to the Hg^{2+} ion, and the broadening of peaks suggests that coordination takes place near the Schiff base and ferrocene moieties. This result indicates that the Hg^{2+} ion could be bound between the amine and Schiff base nitrogen.

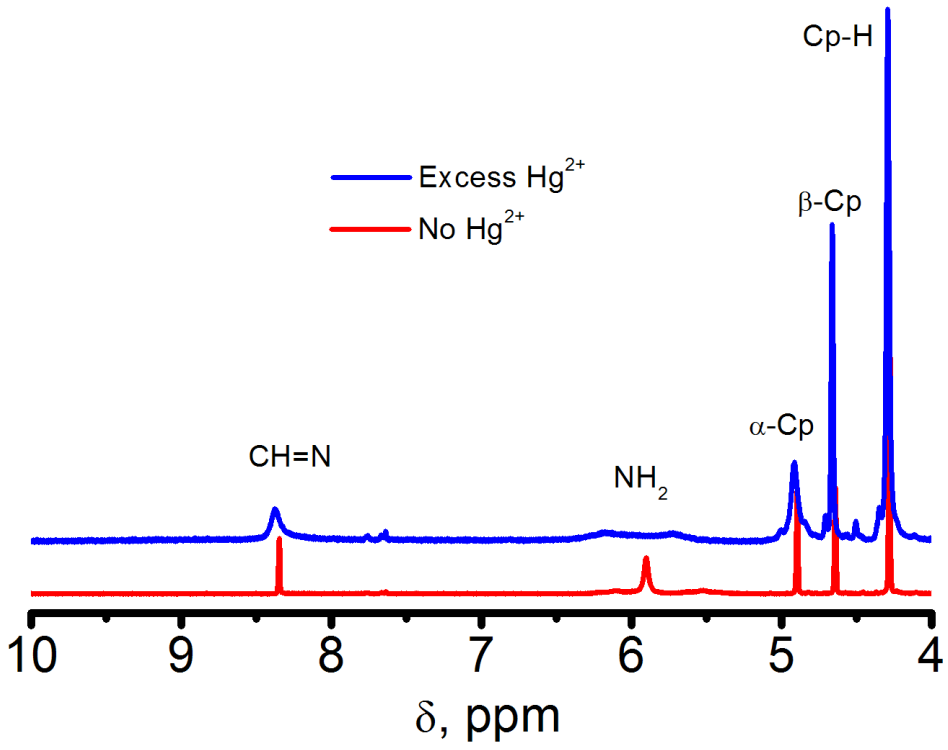

Figure 27. Partial NMR spectra of 1, showing splitting of the amine signal upon fast addition of excess Hg^{2+}.

Ag^+ Recognition. A more complex situation occurs with the interaction between **1** and Ag^+. Increasing the concentration of Ag^+ in acetonitrile solution of **1** also resulted in a red shift of the π - π* band from 362 to 410 nm (Δ = 48 nm) and a flattening of the ICT band (Figure 28). Further addition led to the gradual decay of the π - π* band and loss of the ICT band. The continuous rise of the spectra at higher wavelengths could be due to a

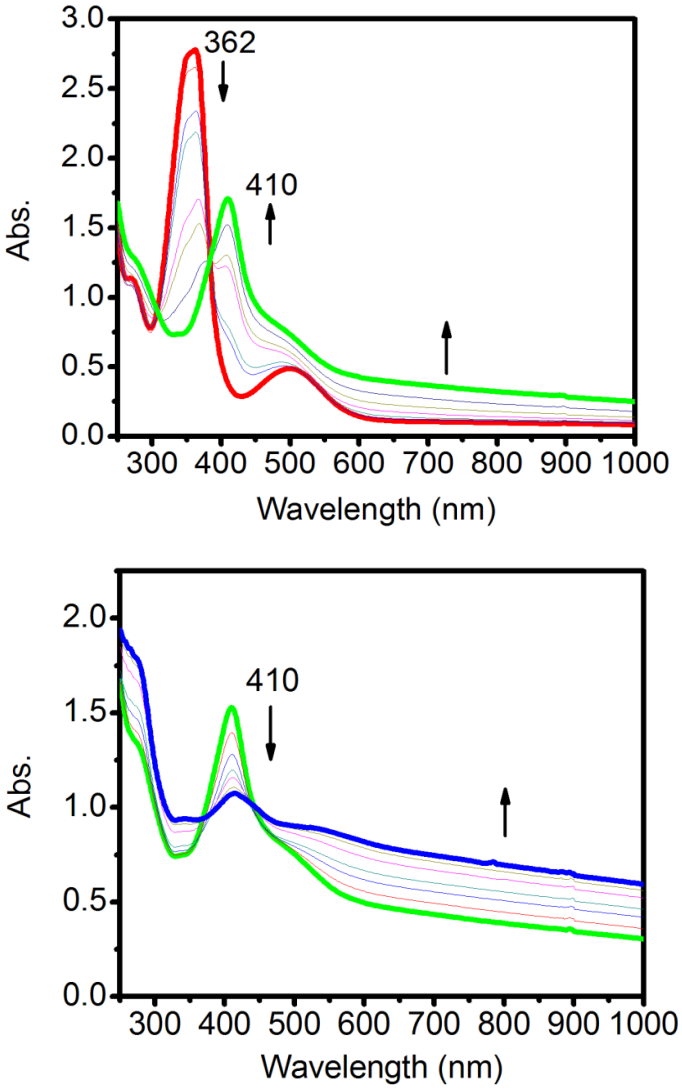

Figure 28. Evolution of absorption spectrum of 1 upon increasing concentration of Ag^+ in acetonitrile solution. Top: 1st process. Bottom: 2nd process.

charge transfer, but no Gaussian- shaped band was observed.

In DCM solution, addition of Ag^+ led to a blue-shift of the ICT band from 509 nm o ~431 nm, and no shift of the π-π* band, similar to the result seen in the spectroelectrochemical oxidation. However, a decrease in intensity of the π-π* was complemented by the rise of a charge transfer band ~900 nm (Figure 29), suggesting that a complexation process has occurred in addition to oxidation.

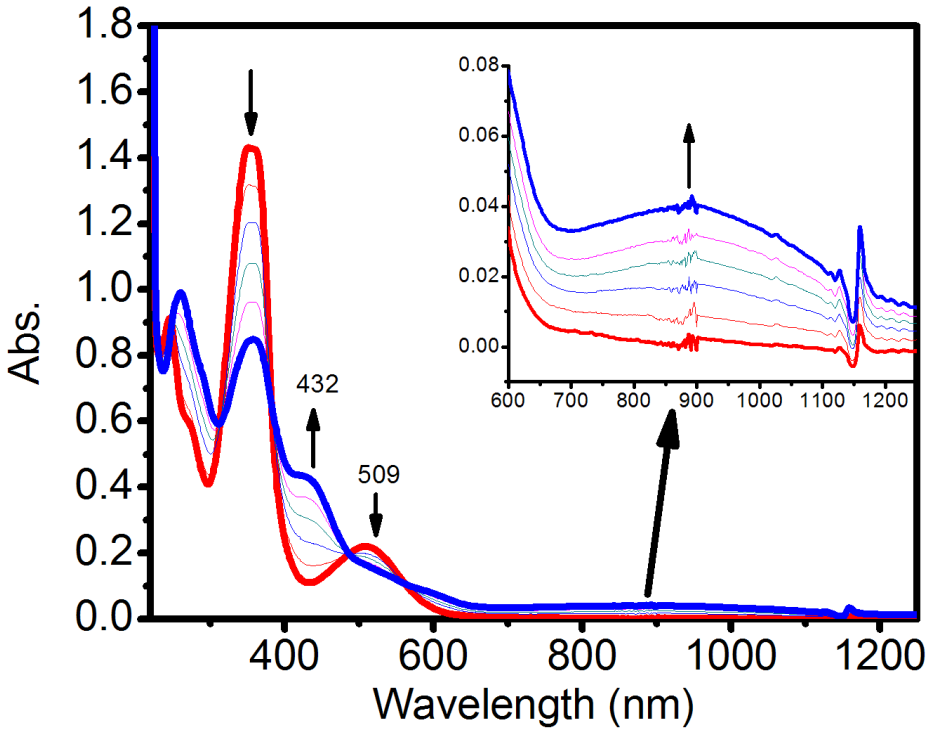

Figure 29. Evolution of absorption spectrum of 1 upon increasing concentration of Ag^+ in dichloromethane solution.

NMR results also seem to suggest two processes. Slowly increasing the concentration of Ag^{+} led to a decrease in the intensity of peaks in the NMR spectrum (Figure 30), while the fast addition of an excess of Ag^{+} let to a splitting of the amine peak, similar to that seen in the Hg^{2+}. Oxidation would result in the formation of a paramagnetic species, undetectable under the standard NMR experiment and thus a reduction of signal, while complexation can explain the split signal. This scenario is further compounded by the known ability of Ag^{+} ions to form complexes with acetonitrile in solution.[53]

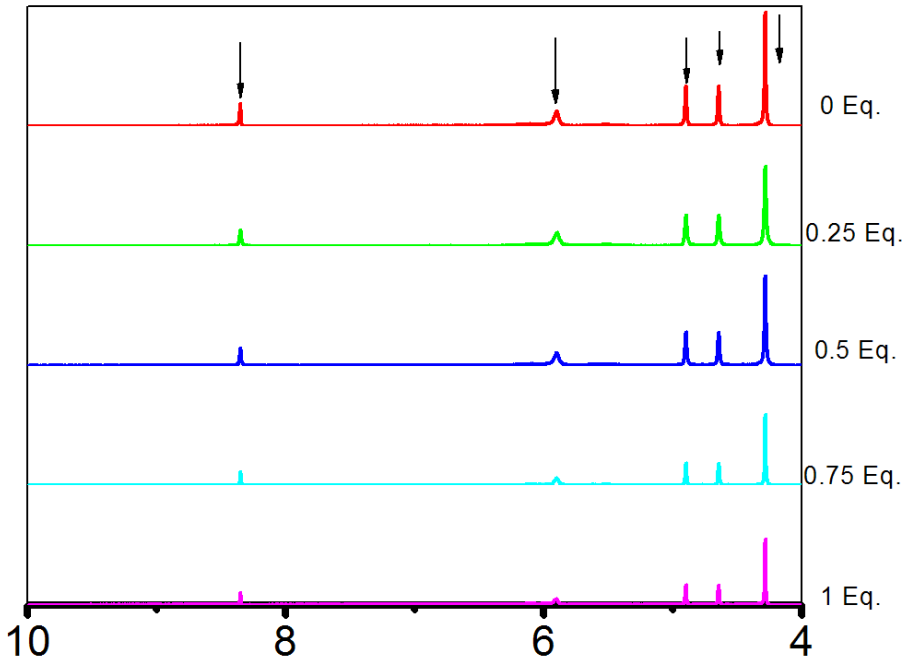

Figure 30. Partial NMR spectra of 1, showing decrease in intensity of signals upon increasing concentration of Ag^{+}.

The addition of metal salts to **2** yielded no shifts in the presence of the test cations except for Ag^{+}. Since the evidence points toward the amine playing a role in coordinating to mercury in the ligand **1**, the lack of this group in **2** would severely hinder its coordination capabilities. Furthermore, if the nitriles aid in coordination, the ligand-metal interactions of **2** would again suffer due to their trans configuration.

4. Conclusions

The condensation products of ferrocene carbaldehyde and diaminomaleonitrile were isolated and their physical structures were determined by ^{1}H NMR, ^{13}C NMR, and IR spectroscopy methods as well as single crystal X-ray diffraction. It was found that the bis-substituted product **2** had rearranged into the trans-isomer, and is thus a fumaronitrile derivative. Upon oxidation to the monocation, the two iron centers were found to communicate via the conjugated π-system, forming a weakly-coupled class II mixed-valence compound. The mono-substituted product **1** was found to selectively interact with Hg^{2+} and Ag^{+} cations. As these ions are known to be toxic, particularly mercury, their detection is of extreme importance and therefore this property is highly sought after for chemosensing applications.

5. References

[1] Kealy, T. J.; Pauson, P.L. *Nature* **1951**, *168*, 1039-1040.

[2] Miller, S. A.; Tebboth, J. A.; Tremaine, J. F. *J. Chem. Soc.* **1952**, 632-635.

[3] Pauson, P.L. *J. Organomet. Chem.* **2001**, *637-639*, 3-6.

[4] (a) Fischer, E. O.; Pfab, W. *Naturforsch* **1952**, *7b*, 377-379. (b) Wilkinson, G.; Rosenblum, M.; Whiting, M. C.; Woodward, R. B. *J. Am. Chem. Soc.* **1952**, *74*, 2125-2126. (c)

[5] Štěpnička, P. Ferrocenes **2008**, John Wiley & Sons, West Sussex, England.

[6] Guzzi, G.P.; La Porta, C.A.M. *Toxicology* **2008**, *244*, 1-12.

[7] Langford, N.J.; Ferner, R.E. *J. Hypertension* **1999**, *13*, 651-656.

[8] Honda, S.; Hylander, L.; Sakamoto M. *Environ. Health Prev. Med.* **2006**, *11*, 171-176

[9] Schroeder, W.H.; Munthe, J. *Atmospheric Environment* **1998**, *32*, 809-822.

[10] (a) Schuster, P. F.; Krabbenhoft, D. P.; Naftz, D. L.; Cecil, L. D.; Olson, M. L.; Dewild, J. F.; Susong, D. D.; Green, J. R.; Abbott, M. L. *Environ. Sci. Technol.*, **2002**, *36*, 2303-2310. (b) Siegel, B. Z.; Siegel, S. M.; Horsky, S. J. *Environ. Sci. Technol.* **1984**, *18*, 179-181. (c) Siegel, S. M.; Siegel, B. Z. *Environ. Sci. Technol.* **1975**, *9*, 473-474

[11] (a) Nolan, E. M.; Lippard, S. J. *Chem. Rev.* **2008**, *108*, 3443-3480. (b) Witherow, R. A.; Lyons, W. B. *Environ. Sci. Technol.* **2008**, *42*, 4710-4716.

[12] Keating, M.H.; Beauregard, D.; Benjey, W.G.; Driver, L.; Maxwell, W.H.; Peters, W.D; Pope, A.A. *Mercury Study Report to Congress* **1997**

[13] Magnuson, J.K.; Anderson, T.N.; Lucht, R.P.; Vijaysarathy, U.A.; Oh, H.; Annamalai, K.; Caton, J.A. *Energy & Fuels* **2008**, *22*, 3029-3036. (b) , Y.; Duan, Y.; Kellie, S.; Li, L.; Xu, W.; Riley, J.T.; Pan, W.P. *Energy & Fuels* **2005**, *19*, 842-854. (c) Drelich, J.; White, C.L.; Xu, Z. *Environ. Sci. Technol.* **2008**, *42*, 2072-2078. (d) Thiebaud, J.; Thomson, M. J.; Mani, R.; Morrow, W.H.; Morris, E.A.; Jia, C.Q. *Environ. Sci. Technol.* **2009**, *43*, 9294-9299. (e) Liu, Y.; Xu, Z.; Kuznicki, S.M.; *Energy & Fuels* **2010**, *24*, 10-17.

[14] Ivask, A.; Hakkila, K.; Virta M. *Anal. Chem.* **2001**, *73*, 5168-5171.

[15] (a) Gantner, N.; Hintelmann, H.; Zheng, W.; Muir, D. C. *Environ. Sci. Technol*. **2009**, *43*, 9148-9154. (b) Feng, X.; Foucher, D.; Hintelmann, H.; Yan, H.; He, T.; Qiu, G. *Envrion. Sci. Technol.* **2010**, *44*, 3363-3368.

[16] (a) Sheng, R.; Wang, P.; Gao, Y.; Wu, Y.; Liu, W.; Ma, J.; Li, H.; Wu, S. *Org. Lett*. **2008**, *10*, 5015-5018. (b) Zhao, Y.; Zhang, X.; Han, Z.; Qiao, L.; Li, C.; Jian, L.; Shen, G.; Yu, R. *Anal. Chem.* **2009**, *81*, 7022-7030. (c) Xu, Z.; Qian, X.; Cui, J. *Org. Lett.* **2005**, *7*, 3029-3032. (d) Lou, X.; Qiang, L.; Qin, J.; Li, Z. *ACS App. Mater. Interfaces* **2009**, *1*, 2529-2535.

[17] (a) Chen, C.; Huang, W. *J. Am. Chem. Soc.* **2002**, *124*, 6246-6247. (b) Kwon, J. Y.; Jang, Y. J.; Lee, Y. J.; Kim, K. M.; Seo, M. S.; Nam, W.; Yoon, J. *J. Am. Chem. Soc.* **2005**, *127*, 10107-10111.

[18] (a) Wang, J.; Huang, L.; Xue, M.; Wang, Y.; Gao, L.; Zhu, J. H.; Zou, Z. *J. Phys. Chem. C* **2008**, *112*, 5014-5022. (b) Xiang, Y.; Tong, A. *Org. Lett.* **2006**, *8*, 1549-1552. (c) Fan, L.; Jones, Jr, W. E. *J. Am. Chem. Soc.* **2006**, *128*, 6784-6785.

[19] (a) Kumar, S.; Luxami, V.; Kumar, A. *Org. Lett.* **2008**, *10*, 5549-5552. (b) Kim S. K.; Bok, J. H.; Bartsch, R. A.; Kim, J. S. *Org. Lett.* **2005**, *7*, 4839-4842. (c) Cho, E. J.; Moon, J. W.; Ko, S. W.; Lee, J. Y.; Kim, S. K.; Yoon, J.; Nam, K. C. *J. Am. Chem. Soc.* **2003**, *125*, 12376-12377.

[20] (a) Ekmekci, Z.; Yilmaz, M. D.; Akkaya, E. U. *Org. Lett.* **2008**, *10*, 461-464. (b) Chen, C.; Chen, Y.; Chen, C.; Sun, S. *Org. Lett.* **2006**, *8*, 5053-5056. (c) Cho, D.; Kim, J. H.; Sessler, J. L. *J. Am. Chem. Soc.* **2008**, *130*, 12163-12167.

[21] (a) Pietrzyk, A.; Suriyanarayanan, S.; Kuther, W.; Chitta, R.; D'Souza, F. *Anal. Chem.* **2009**, *81*, 2633-2643. (b) Chen, H.; Zhao, Q.; Wu, Y.; Li, F.; Yang, H.; Yi, T.; Huang, C. *Inorg. Chem* **2007**, *46*, 11075-11081. (c) Buryak, A.; Severin, K. *J. Am. Chem. Soc.* **2005**, *127*, 3700-3701.

[22] Ojida, A.; Takashima, I.; Kohira, T.; Nonaka, H.; Hamachi, I. *J. Am. Chem. Soc.* **2008**, *130*, 12095-12101.

[23] Lu, H.; Xiong, L.; Liu, H.; Yu, M.; Shen, Z.; Li, F.; You, X. *Org. Biomol. Chem*. **2009**, *7*, 2554-2558.

[24] Chen, X.; Nam, S.; Jou, M. J.; Kim, Y.; Kim, S.; Park, S, Yoon, J. *Org. Lett.* **2008**, *10*, 5235-5238.

[25] (a) Yang, H.; Zhou, Z.; Huang, K.; Yu, M.; Li, F.; Yi, T.; Huang C. *Org. Lett.***2007**, *9*, 4729-4732. (b) Huang, J.; Xu, Y.; Qian X. *J. Org. Chem.***2009**, *74*, 2167-2170. (c) Chun, L.; ZhiGuo, Z.; Yuan, G.; Hong, Y.; BaoGuo, L.; FuYou, L.; ChunHui, H. *Sci. China Ser. B-Chem.* **2009**, *52*, 760-764. (d) Huang, W.; Song, C.; He, C.; Lv, G.;

[26] (a) Kim, S. H.; Youn, N. J.; Park, J. Y.; Choi, M. G.; Chang, S. *Bull. Korean Chem. Soc.* **2006**, *27*, 1553-1556. (b) Kim, H. J.; Kim, S. H.; Kim, J. H.; Lee, E.; Kim, K.; Kim, J. S. *Bull. Korean Chem. Soc.* **2008**, *29*, 1831-1834.

[27] (a) Al-Kady, A. S.; Gaber, M.; Hussein, M. M.; Ebeid, E. M. *J. Phys. Chem.* **2009**, *113*, 9474-9484. (b) Kim, H. J.; Kim, Y.; Kim, S. J.; Park, S. Y.; Lee, S. Y.; Kim, J. H.; No, K.; Kim, J. S. *Bull. Korean Chem. Soc.* **2010**, *31*, 230-233.

[28] Huang, J.; Xu, Y.; Qian, X. *J. Org. Chem.* **2009**, *74*, 2167-2170.

[29] Zhu, M.; Yuan, M.; Liu, X.; Xu, J.; Lv, J.; Huang, C.; Liu, H.; Li, Y.; Wang, S.; Zhu, D. *Org. Lett.* **2008**, *10*, 1481-1484.

[30] Tatay, S.; Gaviña, P.; Coronado, E.; Palomares, E. *Org. Lett.* **2006**, *8*, 3857-3860.

[31] Delavaux-Nicot, B.; Maynadié, J.; Lavabre, D.; Fery-Forgues, S. *Inorg. Chem.* **2006**, *45*, 5691-5702.

[32] (a) Caballero, A.; Espinosa, A.; Tárraga, A.; Molina, P. *J. Org. Chem.* **2008**, *73*, 5489-5497. (b) Yang, H. Zhou, Z.; Huang, K.; Yu, M.; Li, F.; Yi, T.; Huang, C. *Org. Lett.* **2007**, *9*, 4729-4732.

[33] Rahman, M. A.; Son, J. I.; Won, M.; Shim, Y. *Anal. Chem.* **2009**, *81*, 6604-6611.

[34] Robin, M.B.; Day, P. *Adv. Inorg. Chem. Radiochem.* **1967**, *10*, 247-

[35] Creutz, C.; Ford, P.C.; Meyer, T.J. *Inorg. Chem.* **2006**, *45*, 7059-7068.

[36] Shu, P.; Bechgaard, K.; Cowan, D. O. *J. Org. Chem.* **1976**, *41*, 1849-1852.

[37] D'Alessandro, D. M.; Keene, F. R. *Chem. Rev.***2006**, *106*, 2270-2298.

[38] Cowan, D. O.; LeVanda, C.; Park, J.; Kaufman, F *Acc. Chem. Res.* **1973**, *6*, 1-7.

[39] (a) Cowan, D. O.; Kaufman, F. *J. Am. Chem. Soc.* **1970**, *92*, 219-220. (b) Cowan, D. O.; Collins, R. L.; Kaufman, F. *J. Phys. Chem.* **1971**, *75*, 2025-2030.

[40] Kramer, J.A.; Herbstein, F.H.; Hendrickson, D. N. *J. Am. Chem. Soc.* **1980**, *102*, 2293-2301.

[41] Krishnan, A.; Pal, S. K.; Nandakumar, P.; Samuelson, A. G.; Das, P. K. *Chem. Phys.* **2001**, *265*, 313-322.

[42] LeSeur, R.J.; Buttolph, C.; Geiger, W.E.; *Anal Chem.* **2004**, *76*, 6395-6401.

[43] Gaussian 03, Revision C.02, M. J. Frisch, G. W. Trucks, H. B. Schlegel, G. E. Scuseria, M. A. Robb, J. R. Cheeseman, J. A. Montgomery, Jr., T. Vreven, K. N. Kudin, J. C. Burant, J. M. Millam, S. S. Iyengar, J. Tomasi, V. Barone, B. Mennucci, M. Cossi, G. Scalmani, N. Rega, G. A. Petersson, H. Nakatsuji, M. Hada, M. Ehara, K. Toyota, R. Fukuda, J. Hasegawa, M. Ishida, T. Nakajima, Y. Honda, O. Kitao, H. Nakai, M. Klene, X. Li, J. E. Knox, H. P. Hratchian, J. B. Cross, C. Adamo, J. Jaramillo, R. Gomperts, R. E. Stratmann, O. Yazyev, A. J. Austin, R. Cammi, C. Pomelli, J. W. Ochterski, P. Y. Ayala, K. Morokuma, G. A. Voth, P. Salvador, J. J. Dannenberg, V. G. Zakrzewski, S. Dapprich, A. D. Daniels, M. C. Strain, O. Farkas, D. K. Malick, A. D. Rabuck, K. Raghavachari,

J. B. Foresman, J. V. Ortiz, Q. Cui, A. G. Baboul, S. Clifford, J. Cioslowski, B. B. Stefanov, G. Liu, A. Liashenko, P. Piskorz, I. Komaromi, R. L. Martin, D. J. Fox, T. Keith, M. A. Al-Laham, C. Y. Peng, A. Nanayakkara, M. Challacombe, P. M. W. Gill, B. Johnson, W. Chen, M. W. Wong, C. Gonzalez, and J. A. Pople, Gaussian, Inc., Wallingford CT, 2004.

[44] VMOdes Program, Revision A 7.2V. N. Nemykin, P. Basu; University of Minnesota Duluth and Duquesne University; 2001, 2003, 2005.

[45] Yamada, Y.; Nagashima, N.; Iwashita, Y.; Nakamura, A.; Kumashiro, I. *Tetrahedron Lett.* **1968**, *9*, 4529-4532.

[46] Begland, R. W.; Hartter, D. R.; Jones, F. N.; Sam, D. J.; Sheppard, W. A.; Webster, O. W.; Weigert, F. J. *J. Org. Chem.* **1974**, *39*, 2341-2350.

[47] Mak, T. C. W.; Zhou, G. Crystallography in modern chemisty: a resource book of crystal structures. 1992, John Wiley & Sons, New York.

[48] (a) Nemykin, V. N.; Makarova, E. A.; Grosland, J. O.; Hadt, R. G.; Koposov, A. Y. *Inorg. Chem.* **2007**, *46*, 9591-9601. (b) Hess, A.; Sehnert, J.; Weyhermüller, T.; Metzler-Nolte, N. *Inorg. Chem.* **2000**, *39*, 5437-5443. (c) Caballero, A.; Llovera, V.; Curiel, D.; Tárraga, A.; Espinosa, A.; García, R.; Vidal-Gancedo, J.; Rovira, C.; Wurst, K.; Molina, P.; Veciana, J. *Inorg. Chem.* **2007**, *46*, 825-838.

[49] Mayor-López, M.; Weber, J. *Organometallics* **1998**, *17*, 4983-4991.

[50] Cowan, D. O.; Candela, G. A.; Kaufman, F. *J. Am. Chem. Soc.* **1971**, *93*, 3889-3893.

[51] Penfold, B. R.; Lipscomb, W. N. *Acta. Cryst.* **1961**, *14*, 589-597.

[52] Marcus, Y. *Chem. Soc. Rev.* **1993**, *22*, 409-416.

[53] Connelly, N. G.; Geiger, W. E. *Chem. Rev.* **1996**, *96*, 877-910.

6. Supplemental Information

6.1 CIF file for 1

X-ray Structure Report

for

_04_20_2010_01_red

June 11, 2010

Experimental

Data Collection

A colorless prism crystal of $C_{40}H_{20}FeN_4$ having approximate dimensions of 0.20 x 0.20 x 0.20 mm was mounted on a glass fiber. All measurements were made on a Rigaku RAXIS-UNKNOWN diffractometer using graphite monochromated Mo-Kα radiation.

The crystal-to-detector distance was 127.40 mm.

Cell constants and an orientation matrix for data collection corresponded to a primitive monoclinic cell with dimensions:

a = 10.9199(4) Å

b = 11.1511(3) Å β = 110.413(8)°

c = 11.7006(8) Å

V = 1335.30(13) $Å^3$

For Z = 2 and F.W. = 612.47, the calculated density is 1.523 g/cm^3. The reflection conditions of:

h0l: l = 2n

0k0: k = 2n

uniquely determine the space group to be:

$P2_1/c$ (#14)

The data were collected at a temperature of -160 ± 1°C to a maximum 2θ value of 55.0°. A total of 42 oscillation images were collected. A sweep of data was done using ω oscillations from 20.0 to 170.0° in 5.0° steps. The exposure rate was 180.0 [sec./°]. A second sweep was performed using ω oscillations from 35.0 to 95.0° in 5.0° steps. The exposure rate was 180.0 [sec./°]. Another sweep was performed using ω oscillations from 20.0 to 170.0° in 5.0° steps. The exposure rate was 180.0 [sec./°]. Another sweep was performed using ω oscillations from 35.0 to 95.0° in 5.0° steps. The exposure rate was 180.0 [sec./°]. The crystal-to-detector distance was 127.40 mm. Readout was performed in the 0.100 mm pixel mode.

Data Reduction

Of the 12079 reflections that were collected, 3051 were unique (R_{int} = 0.031).

The linear absorption coefficient, μ, for Mo-Kα radiation is 6.047 cm^{-1}. An empirical absorption correction was applied which resulted in transmission factors ranging from 0.632 to 0.886. The data were corrected for Lorentz and polarization effects.

Structure Solution and Refinement

The structure was solved by direct methods[1] and expanded using Fourier techniques. The non-hydrogen atoms were refined anisotropically. Hydrogen atoms were refined using the riding model. The final cycle of full-matrix least-squares refinement[2] on F^2 was based on 3051 observed reflections and 255 variable parameters and converged (largest parameter shift was 1.52 times its esd) with unweighted and weighted agreement factors of:

$$R1 = \Sigma \; ||Fo| - |Fc|| \; / \; \Sigma \; |Fo| = 0.0297$$

$$wR2 = [\; \Sigma \; (\; w \; (Fo^2 - Fc^2)^2 \;) / \; \Sigma \; w(Fo^2)^2]^{1/2} = 0.0810$$

The standard deviation of an observation of unit weight[3] was 1.09. Unit weights were used. The maximum and minimum peaks on the final difference Fourier map corresponded to 0.43 and -0.38 $e^-/Å^3$, respectively.

Neutral atom scattering factors were taken from Cromer and Waber[4]. Anomalous dispersion effects were included in Fcalc[5]; the values for Δf' and Δf'' were those of Creagh and McAuley[6]. The values for the mass attenuation coefficients are those of Creagh and Hubbell[7]. All calculations were performed using the CrystalStructure[8] crystallographic software package except for refinement, which was performed using SHELXL-97[9].

References

(1) SHELX97: Sheldrick, G.M. (1997).

(2) Least Squares function minimized: (SHELXL97)

$\Sigma w(F_o^2-F_c^2)^2$ where w = Least Squares weights.

(3) Standard deviation of an observation of unit weight:

$[\Sigma w(F_o^2-F_c^2)^2/(N_o-N_v)]^{1/2}$

where: N_o = number of observations

N_v = number of variables

(4) Cromer, D. T. & Waber, J. T.; "International Tables for X-ray Crystallography", Vol. IV, The Kynoch Press, Birmingham, England, Table 2.2 A (1974).

(5) Ibers, J. A. & Hamilton, W. C.; Acta Crystallogr., 17, 781 (1964).

(6) Creagh, D. C. & McAuley, W.J .; "International Tables for Crystallography", Vol C, (A.J.C. Wilson, ed.), Kluwer Academic Publishers, Boston, Table 4.2.6.8, pages 219-222 (1992).

(7) Creagh, D. C. & Hubbell, J.H..; "International Tables for Crystallography", Vol C, (A.J.C. Wilson, ed.), Kluwer Academic Publishers, Boston, Table 4.2.4.3, pages 200-206 (1992).

(8) CrystalStructure 4.0: Crystal Structure Analysis Package, Rigaku and Rigaku Americas (2000-2009). 9009 New Trails Dr. The Woodlands TX 77381 USA.

(9) SHELX97: Sheldrick, G.M. (1997).

EXPERIMENTAL DETAILS

A. Crystal Data

Empirical Formula	$C_{40}H_{20}FeN_4$
Formula Weight	612.47
Crystal Color, Habit	colorless, prism
Crystal Dimensions	0.20 X 0.20 X 0.20 mm

Crystal System	monoclinic
Lattice Type	Primitive
Lattice Parameters	a = 10.9199(4) Å
	b = 11.1511(3) Å
	c = 11.7006(8) Å
	β = 110.413(8) ^{o}
	V = 1335.30(13) Å^{3}
Space Group	$P2_1/c$ (#14)
Z value	2
D_{calc}	1.523 g/cm^{3}
F_{000}	628.00
□(MoK□)	6.047 cm^{-1}

B. Intensity Measurements

Diffractometer	Rigaku RAXIS-UNKNOWN
Radiation	MoKα (λ = 0.71075 Å)
	graphite monochromated
Voltage, Current	50kV, 40mA
Temperature	-160.0^{o}C
Detector Aperture	280 x 256 mm
Data Images	42 exposures
ω oscillation Range	20.0 - 170.0^{o}
Exposure Rate	180.0 sec./^{o}
ω oscillation Range	35.0 - 95.0^{o}
Exposure Rate	180.0 sec./^{o}

ω oscillation Range	20.0 - 170.0^{o}
Exposure Rate	180.0 sec./^{o}
ω oscillation Range	35.0 - 95.0^{o}
Exposure Rate	180.0 sec./^{o}
Detector Position	127.40 mm
Pixel Size	0.100 mm
$2\theta_{max}$	55.0^{o}
No. of Reflections Measured	Total: 12079
	Unique: 3051 (R_{int} = 0.031)
Corrections	Lorentz-polarization
	Absorption
	(trans. factors: 0.632 - 0.886)

C. Structure Solution and Refinement

Structure Solution	Direct Methods (SHELX97)
Refinement	Full-matrix least-squares on F^2
Function Minimized	Σ w (Fo^2 - Fc^2)^2
Least Squares Weights	w = 1/ [$\sigma^2(Fo^2)$ + (0.0320 · P)^2
	+ 1.3977 · P]
	where P = (Max(Fo^2,0) + 2Fc^2)/3
$2\theta_{max}$ cutoff	55.0^{o}
Anomalous Dispersion	All non-hydrogen atoms
No. Observations (All reflections)	3051
No. Variables	255
Reflection/Parameter Ratio	11.96

Residuals: R1 (I>2.00σ(I))	0.0297
Residuals: R (All reflections)	0.0384
Residuals: wR2 (All reflections)	0.0810
Goodness of Fit Indicator	1.086
Max Shift/Error in Final Cycle	1.524
Maximum peak in Final Diff. Map	0.43 $e^-/Å^3$
Minimum peak in Final Diff. Map	-0.38 $e^-/Å^3$

Table 1. Atomic coordinates and B_{iso}/B_{iso}

atom	x	y	z	B_{eq}
Fe(1)	0.61942(3)	0.82059(2)	0.17029(3)	1.159
N(2)	1.09253(19)	0.78367(17)	0.64209(19)	1.706
N(3)	0.88384(16)	0.90556(15)	0.47869(15)	1.302
N(5)	0.78994(19)	1.08126(18)	0.68161(18)	2.083
N(15)	1.0795(2)	0.87177(19)	0.91502(18)	2.308
C(4)	0.78724(19)	0.96138(17)	0.40089(17)	1.223
C(6)	0.91720(19)	0.92539(18)	0.60376(18)	1.357
C(7)	0.6002(2)	0.65623(19)	0.2406(2)	1.805
C(8)	0.6595(2)	1.00038(19)	0.1727(2)	1.334
C(9)	0.8493(2)	1.01109(19)	0.65080(18)	1.542
C(11)	1.01994(19)	0.86031(18)	0.68041(18)	1.449
C(12)	0.75661(18)	0.94003(17)	0.27153(18)	1.213
C(13)	0.5365(3)	0.7462(2)	0.2856(2)	1.891
C(16)	1.0541(2)	0.87139(19)	0.81163(19)	1.594
C(17)	0.7568(2)	0.8575(2)	0.0908(2)	1.424

C(18)	0.4409(2)	0.7434(2)	0.0764(2)	1.853
C(19)	0.6604(2)	0.94932(18)	0.0619(2)	1.322
C(20)	0.5410(2)	0.65472(19)	0.1115(2)	1.704
C(21)	0.8160(2)	0.85062(19)	0.21981(19)	1.316
C(22)	0.4381(2)	0.8000(2)	0.1845(2)	1.853

$B_{eq} = 8/3\ \pi^2(U_{11}(aa^*)^2 + U_{22}(bb^*)^2 + U_{33}(cc^*)^2 + 2U_{12}(aa^*bb^*)\cos\gamma + 2U_{13}(aa^*cc^*)\cos\beta + 2U_{23}(bb^*cc^*)\cos\alpha)$

Table 2. Atomic coordinates and B_{iso}/B_{eq} involving hydrogen atoms

atom	x	y	z	B_{eq}
H(4)	0.7364	1.0161	0.4280	1.47
H(8)	0.606(2)	1.059(2)	0.181(2)	1.863
H(10)	0.668(3)	0.611(2)	0.284(3)	2.5(6)
H(13)	0.558(3)	0.767(2)	0.361(3)	3.285
H(14)	0.566(2)	0.607(2)	0.062(2)	1.4(5)
H(17)	0.779(2)	0.809(2)	0.040(3)	2.184
H(19)	0.609(2)	0.972(2)	-0.018(2)	1.599
H(21)	0.882(2)	0.796(2)	0.266(2)	2.103
H(22)	0.384(3)	0.861(2)	0.191(2)	2.276
H(23)	0.388(3)	0.761(2)	-0.004(2)	2.3(5)
H(24)	1.066(3)	0.766(2)	0.568(3)	2.3(6)
H(26)	1.141(3)	0.738(3)	0.690(3)	2.2(6)

$B_{eq} = 8/3\ \pi^2(U_{11}(aa^*)^2 + U_{22}(bb^*)^2 + U_{33}(cc^*)^2 + 2U_{12}(aa^*bb^*)\cos\gamma + 2U_{13}(aa^*cc^*)\cos\beta + 2U_{23}(bb^*cc^*)\cos\alpha$

Table 3. Anisotropic displacement parameters

atom	U_{11}	U_{22}	U_{33}	U_{12}	U_{13}	U_{23}
Fe(1)	0.0158	0.0139	0.0144	-0.0007	0.0054	-0.0001
N(2)	0.0234	0.0219	0.0164	0.0029	0.0030	0.0005
N(3)	0.0181	0.0165	0.0146	-0.0026	0.0054	0.0005
N(5)	0.0272	0.0288	0.0242	-0.0022	0.0103	-0.0074
N(15)	0.0331	0.0325	0.0203	-0.0078	0.0070	0.0008
C(4)	0.0184	0.0158	0.0139	-0.0022	0.0078	-0.0017
C(6)	0.0193	0.0178	0.0150	-0.0043	0.0066	-0.0030
C(7)	0.0259	0.0165	0.0259	-0.0019	0.0086	0.0036
C(8)	0.0168	0.0121	0.0217	0.0028	0.0066	0.0008
C(9)	0.0207	0.0235	0.0134	-0.0059	0.0047	-0.0029
C(11)	0.0199	0.0185	0.0159	-0.0060	0.0054	-0.0012
C(12)	0.0144	0.0157	0.0153	-0.0014	0.0044	-0.0005
C(13)	0.0278	0.0241	0.0234	-0.0088	0.0132	-0.0009
C(16)	0.0224	0.0191	0.0173	-0.0059	0.0047	0.0015
(17)	0.0176	0.0183	0.0198	0.0001	0.0086	0.0010
C(18)	0.0219	0.0249	0.0215	-0.0090	0.0049	-0.0009
C(19)	0.0181	0.0183	0.0137	-0.0010	0.0054	0.0016
C(20)	0.0280	0.0175	0.0210	-0.0078	0.0108	-0.0062
C(21)	0.0159	0.0182	0.0160	0.0005	0.0056	-0.0019
C(22)	0.0208	0.0185	0.0349	-0.0033	0.0144	-0.0003

The general temperature factor expression: $\exp(-2\pi^2(a^{*2}U_{11}h^2 + b^{*2}U_{22}k^2 + c^{*2}U_{33}l^2 + 2a^*b^*U_{12}hk + 2a^*c^*U_{13}hl + 2b^*c^*U_{23}kl))$

Table 4. Bond lengths (Å)

atom	atom	distance	atom	atom	distance
Fe(1)	C(7)	2.050(3)	Fe(1)	C(8)	2.050(3)
Fe(1)	C(12)	2.045(3)	Fe(1)	C(13)	2.044(4)
Fe(1)	C(17)	2.064(3)	Fe(1)	C(18)	2.062(4)
Fe(1)	C(19)	2.065(3)	Fe(1)	C(20)	2.053(4)
Fe(1)	C(21)	2.047(3)	Fe(1)	C(22)	2.057(4)
N(2)	C(11)	1.344(3)	N(3)	C(4)	1.2880(16)
N(3)	C(6)	1.397(3)	N(5)	C(9)	1.151(3)
N(15)	C(16)	1.143(3)	C(4)	C(12)	1.451(4)
C(6)	C(9)	1.432(3)	C(6)	C(11)	1.3740(18)
C(7)	C(13)	1.422(4)	C(7)	C(20)	1.421(4)
C(8)	C(12)	1.435(2)	C(8)	C(19)	1.419(5)
C(11)	C(16)	1.453(4)	C(12)	C(21)	1.433(3)
C(13)	C(22)	1.424(3)	C(17)	C(19)	1.422(2)
C(17)	C(21)	1.422(4)	C(18)	C(20)	1.424(2)
C(18)	C(22)	1.424(5)			

Table 5. Bond lengths involving hydrogens (Å)

atom	atom	distance	atom	atom	distance
N(2)	H(24)	0.83(3)	N(2)	H(26)	0.805(15)
C(4)	H(4)	0.950	C(7)	H(10)	0.90(2)
C(8)	H(8)	0.91(2)	C(13)	H(13)	0.87(4)
C(17)	H(17)	0.90(3)	C(18)	H(23)	0.93(2)

C(19)	H(19)	0.940(19)	C(20)	H(14)	0.90(2)
C(21)	H(21)	0.958(15)	C(22)	H(22)	0.92(2)

Table 6. Bond angles (°)

atom	atom	atom	angle	atom	atom	atom	angle
C(7)	Fe(1)	C(8)	156.96(10)	C(7)	Fe(1)	C(12)	120.43(8)
C(7)	Fe(1)	C(13)	40.67(11)	C(7)	Fe(1)	C(17)	123.48(10)
C(7)	Fe(1)	C(18)	68.32(8)	C(7)	Fe(1)	C(19)	160.49(10)
C(7)	Fe(1)	C(20)	40.52(9)	C(7)	Fe(1)	C(21)	106.06(9)
C(7)	Fe(1)	C(22)	68.37(10)	C(8)	Fe(1)	C(12)	41.03(7)
C(8)	Fe(1)	C(13)	121.94(11)	C(8)	Fe(1)	C(17)	68.03(10)
C(8)	Fe(1)	C(18)	124.96(8)	C(8)	Fe(1)	C(19)	40.33(10)
C(8)	Fe(1)	C(20)	161.35(8)	C(8)	Fe(1)	C(21)	68.80(9)
C(8)	Fe(1)	C(22)	108.36(10)	C(12)	Fe(1)	C(13)	106.57(9)
C(12)	Fe(1)	C(17)	68.31(9)	C(12)	Fe(1)	C(18)	161.00(9)
C(12)	Fe(1)	C(19)	68.35(8)	C(12)	Fe(1)	C(20)	156.37(8)
C(12)	Fe(1)	C(21)	41.01(9)	C(12)	Fe(1)	C(22)	123.86(10)
C(13)	Fe(1)	C(17)	159.59(9)	C(13)	Fe(1)	C(18)	68.19(10)
C(13)	Fe(1)	C(19)	158.11(10)	C(13)	Fe(1)	C(20)	68.08(10)
C(13)	Fe(1)	C(21)	122.80(9)	C(13)	Fe(1)	C(22)	40.62(9)
C(17)	Fe(1)	C(18)	122.94(10)	C(17)	Fe(1)	C(19)	40.29(9)
C(17)	Fe(1)	C(20)	108.22(10)	C(17)	Fe(1)	C(21)	40.48(8)
C(17)	Fe(1)	C(22)	158.50(9)	C(18)	Fe(1)	C(19)	109.29(9)
C(18)	Fe(1)	C(20)	40.47(9)	C(18)	Fe(1)	C(21)	157.26(10)
C(18)	Fe(1)	C(22)	40.43(10)	C(19)	Fe(1)	C(20)	125.10(9)

C(19)	Fe(1)	C(21)	68.24(8)	C(19)	Fe(1)	C(22)	123.26(9)
C(20)	Fe(1)	C(21)	121.07(9)	C(20)	Fe(1)	C(22)	68.01(10)
C(21)	Fe(1)	C(22)	159.99(10)	C(4)	N(3)	C(6)	120.93(19)
N(3)	C(4)	C(12)	119.46(19)	N(3)	C(6)	C(9)	121.83(16)
N(3)	C(6)	C(11)	117.09(20)	C(9)	C(6)	C(11)	121.07(19)
Fe(1)	C(7)	C(13)	69.46(15)	Fe(1)	C(7)	C(20)	69.88(13)
C(13)	C(7)	C(20)	107.55(19)	Fe(1)	C(8)	C(12)	69.31(11)
Fe(1)	C(8)	C(19)	70.41(12)	C(12)	C(8)	C(19)	108.00(19)
N(5)	C(9)	C(6)	175.94(20)	N(2)	C(11)	C(6)	124.07(20)
N(2)	C(11)	C(16)	116.26(17)	C(6)	C(11)	C(16)	119.7(2)
Fe(1)	C(12)	C(4)	124.52(16)	Fe(1)	C(12)	C(8)	69.66(11)
Fe(1)	C(12)	C(21)	69.54(11)	C(4)	C(12)	C(8)	126.89(20)
C(4)	C(12)	C(21)	125.50(16)	C(8)	C(12)	C(21)	107.57(18)
Fe(1)	C(13)	C(7)	69.87(16)	Fe(1)	C(13)	C(22)	70.18(16)
C(7)	C(13)	C(22)	108.3(2)	N(15)	C(16)	C(11)	175.3(2)
Fe(1)	C(17)	C(19)	69.92(15)	Fe(1)	C(17)	C(21)	69.12(15)
C(19)	C(17)	C(21)	108.4(2)	Fe(1)	C(18)	C(20)	69.42(12)
Fe(1)	C(18)	C(22)	69.58(12)	C(20)	C(18)	C(22)	107.68(18)
Fe(1)	C(19)	C(8)	69.27(14)	Fe(1)	C(19)	C(17)	69.80(14)
C(8)	C(19)	C(17)	108.23(18)	Fe(1)	C(20)	C(7)	69.59(12)
Fe(1)	C(20)	C(18)	70.10(12)	C(7)	C(20)	C(18)	108.5(2)
Fe(1)	C(21)	C(12)	69.45(12)	Fe(1)	C(21)	C(17)	70.40(13)
C(12)	C(21)	C(17)	107.79(18)	Fe(1)	C(22)	C(13)	69.20(16)
Fe(1)	C(22)	C(18)	69.98(15)	C(13)	C(22)	C(18)	107.9(2)

Table 7. Bond angles involving hydrogens (°)

atom	atom	atom	angle	atom	atom	atom	angle
C(11)	N(2)	H(24)	118.0(19)	C(11)	N(2)	H(26)	120(2)
H(24)	N(2)	H(26)	118(3)	N(3)	C(4)	H(4)	120
C(12)	C(4)	H(4)	120	Fe(1)	C(7)	H(10)	123.8(19)
C(13)	C(7)	H(10)	127.3(19)	C(20)	C(7)	H(10)	125.1(20)
Fe(1)	C(8)	H(8)	124.6(17)	C(12)	C(8)	H(8)	124.8(14)
C(19)	C(8)	H(8)	127.2(13)	Fe(1)	C(13)	H(13)	123(2)
C(7)	C(13)	H(13)	125.2(18)	C(22)	C(13)	H(13)	126.4(18)
Fe(1)	C(17)	H(17)	125.5(17)	C(19)	C(17)	H(17)	128.6(15)
C(21)	C(17)	H(17)	123.0(15)	Fe(1)	C(18)	H(23)	126.1(18)
C(20)	C(18)	H(23)	125.5(19)	C(22)	C(18)	H(23)	126.8(19)
Fe(1)	C(19)	H(19)	128.1(16)	C(8)	C(19)	H(19)	127.1(17)
C(17)	C(19)	H(19)	124.6(17)	Fe(1)	C(20)	H(14)	124.2(16)
C(7)	C(20)	H(14)	124.5(14)	C(18)	C(20)	H(14)	127.0(14)
Fe(1)	C(21)	H(21)	124.3(16)	C(12)	C(21)	H(21)	124.8(16)
C(17)	C(21)	H(21)	127.4(16)	Fe(1)	C(22)	H(22)	126.2(18)
C(13)	C(22)	H(22)	124.4(16)	C(18)	C(22)	H(22)	127.6(16)

Table 8. Torsion Angles(°)

(Those having bond angles > 160 degrees are excluded.)

atom1	atom2	atom3	atom4	angle	atom1 atom2 atom3 atom4 angle
C(7)	Fe(1)	C(8)	C(12)	43.1(3)	C(7) Fe(1) C(8) C(19) 162.1(2)
C(8)	Fe(1)	C(7)	C(13)	48.5(3)	C(8) Fe(1) C(7) C(20) 167.2(2)
C(7)	Fe(1)	C(12)	C(4)	-40.5(2)	C(7) Fe(1) C(12) C(8) -161.93(15)
C(7)	Fe(1)	C(12)	C(21)	79.25(16)	C(12) Fe(1) C(7) C(13) 79.86(15)
C(12)	Fe(1)	C(7)	C(20)	-161.45(14)	C(7) Fe(1) C(13) C(7) 0
C(7)	Fe(1)	C(13)	C(22)	-119.23(19)	C(13) Fe(1) C(7) C(13) 0
C(13)	Fe(1)	C(7)	C(20)	118.69(19)	C(7) Fe(1) C(17) C(19) 165.35(12)
C(7)	Fe(1)	C(17)	C(21)	-74.70(15)	C(17) Fe(1) C(7) C(13) 162.65(12)
C(17)	Fe(1)	C(7)	C(20)	-78.66(16)	C(7) Fe(1) C(18) C(20) -37.41(15)
C(7)	Fe(1)	C(18)	C(22)	81.67(15)	C(18) Fe(1) C(7) C(13) -81.33(14)
C(18)	Fe(1)	C(7)	C(20)	37.36(15)	C(7) Fe(1) C(20) C(7) 0
C(7)	Fe(1)	C(20)	C(18)	119.7(2)	C(20) Fe(1) C(7) C(13) -118.69(19)
C(20)	Fe(1)	C(7)	C(20)	0	C(7) Fe(1) C(21) C(12) -118.17(13)
C(7)	Fe(1)	C(21)	C(17)	123.15(14)	C(21) Fe(1) C(7) C(13) 121.99(13)
C(21)	Fe(1)	C(7)	C(20)	-119.31(15)	C(7) Fe(1) C(22) C(13) 37.71(15)
C(7)	Fe(1)	C(22)	C(18)	-81.52(14)	C(22) Fe(1) C(7) C(13) -37.67(13)
C(22)	Fe(1)	C(7)	C(20)	81.02(15)	C(8) Fe(1) C(12) C(4) 121.5(2)
C(8)	Fe(1)	C(12)	C(8)	0	C(8) Fe(1) C(12) C(21) -118.81(20)
C(12)	Fe(1)	C(8)	C(12)	0	C(12) Fe(1) C(8) C(19) 119.01(19)
C(8)	Fe(1)	C(13)	C(7)	-159.79(11)	C(8) Fe(1) C(13) C(22) 80.98(16)
C(13)	Fe(1)	C(8)	C(12)	78.21(16)	C(13) Fe(1) C(8) C(19) -162.78(12)
C(8)	Fe(1)	C(17)	C(19)	-37.31(12)	C(8) Fe(1) C(17) C(21) 82.65(13)

C(17)	Fe(1)	C(8)	C(12)	-81.75(14)	C(17) Fe(1) C(8) C(19) 37.27(12)
C(8)	Fe(1)	C(18)	C(20)	164.10(15)	C(8) Fe(1) C(18) C(22) -76.82(17)
C(18)	Fe(1)	C(8)	C(12)	162.57(14)	C(18) Fe(1) C(8) C(19) -78.42(16)
C(8)	Fe(1)	C(19)	C(8)	0	C(8) Fe(1) C(19) C(17) 119.71(16)
C(19)	Fe(1)	C(8)	C(12)	-119.01(19)	C(19) Fe(1) C(8) C(19) 0
C(8)	Fe(1)	C(21)	C(12)	38.09(13)	C(8) Fe(1) C(21) C(17) -80.58(14)
C(21)	Fe(1)	C(8)	C(12)	-38.08(14)	C(21) Fe(1) C(8) C(19) 80.94(13)
C(8)	Fe(1)	C(22)	C(13)	-117.99(15)	C(8) Fe(1) C(22) C(18) 122.78(13)
C(22)	Fe(1)	C(8)	C(12)	120.86(15)	C(22) Fe(1) C(8) C(19) -120.13(13)
C(12)	Fe(1)	C(13)	C(7)	-117.68(12)	C(12) Fe(1) C(13) C(22) 123.09(14)
C(13)	Fe(1)	C(12)	C(4)	1.54(19)	C(13) Fe(1) C(12) C(8) -119.92(16)
C(13)	Fe(1)	C(12)	C(21)	121.26(14)	C(12) Fe(1) C(17) C(19) -81.67(12)
C(12)	Fe(1)	C(17)	C(21)	38.29(12)	C(17) Fe(1) C(12) C(4) -157.52(18)
C(17)	Fe(1)	C(12)	C(8)	81.01(15)	C(17) Fe(1) C(12) C(21) -37.80(13)
C(12)	Fe(1)	C(19)	C(8)	-38.15(12)	C(12) Fe(1) C(19) C(17) 81.57(13)
C(19)	Fe(1)	C(12)	C(4)	158.98(19)	C(19) Fe(1) C(12) C(8) 37.51(15)
C(19)	Fe(1)	C(12)	C(21)	-81.30(14)	C(12) Fe(1) C(20) C(7) 43.2(3)
C(12)	Fe(1)	C(20)	C(18)	162.9(2)	C(20) Fe(1) C(12) C(4) -71.5(3)
C(20)	Fe(1)	C(12)	C(8)	167.0(2)	C(20) Fe(1) C(12) C(21) 48.2(3)
C(12)	Fe(1)	C(21)	C(12)	0	C(12) Fe(1) C(21) C(17) -118.67(18)
C(21)	Fe(1)	C(12)	C(4)	-119.7(2)	C(21) Fe(1) C(12) C(8) 118.81(20)
C(21)	Fe(1)	C(12)	C(21)	0	C(12) Fe(1) C(22) C(13) -75.25(16)
C(12)	Fe(1)	C(22)	C(18)	165.51(12)	C(22) Fe(1) C(12) C(4) 42.61(19)
C(22)	Fe(1)	C(12)	C(8)	-78.86(17)	C(22) Fe(1) C(12) C(21) 162.33(13)
C(13)	Fe(1)	C(17)	C(19)	-160.8(2)	C(13) Fe(1) C(17) C(21) -40.8(3)
C(17)	Fe(1)	C(13)	C(7)	-45.5(3)	C(17) Fe(1) C(13) C(22) -164.7(2)

C(13)	Fe(1)	C(18)	C(20)	-81.35(16)	C(13) Fe(1) C(18) C(22) 37.73(14)
C(18)	Fe(1)	C(13)	C(7)	81.67(13)	C(18) Fe(1) C(13) C(22) -37.56(14)
C(13)	Fe(1)	C(19)	C(8)	42.4(3)	C(13) Fe(1) C(19) C(17) 162.1(2)
C(19)	Fe(1)	C(13)	C(7)	169.29(19)	C(19) Fe(1) C(13) C(22) 50.1(3)
C(13)	Fe(1)	C(20)	C(7)	-38.04(15)	C(13) Fe(1) C(20) C(18) 81.64(16)
C(20)	Fe(1)	C(13)	C(7)	37.91(12)	C(20) Fe(1) C(13) C(22) -81.32(15)
C(13)	Fe(1)	C(21)	C(12)	-77.07(15)	C(13) Fe(1) C(21) C(17) 164.26(14)
C(21)	Fe(1)	C(13)	C(7)	-75.82(15)	C(21) Fe(1) C(13) C(22) 164.94(13)
C(13)	Fe(1)	C(22)	C(13)	0	C(13) Fe(1) C(22) C(18) -119.23(20)
C(22)	Fe(1)	C(13)	C(7)	119.23(19)	C(22) Fe(1) C(13) C(22) 0
C(17)	Fe(1)	C(18)	C(20)	79.31(17)	C(17) Fe(1) C(18) C(22) -161.61(13)
C(18)	Fe(1)	C(17)	C(19)	81.04(14)	C(18) Fe(1) C(17) C(21) -159.00(12)
C(17)	Fe(1)	C(19)	C(8)	-119.71(16)	C(17) Fe(1) C(19) C(17) 0
C(19)	Fe(1)	C(17)	C(19)	0	C(19) Fe(1) C(17) C(21) 119.96(18)
C(17)	Fe(1)	C(20)	C(7)	120.57(15)	C(17) Fe(1) C(20) C(18) -119.75(15)
C(20)	Fe(1)	C(17)	C(19)	123.22(12)	C(20) Fe(1) C(17) C(21) -116.82(13)
C(17)	Fe(1)	C(21)	C(12)	118.67(18)	C(17) Fe(1) C(21) C(17) -0
C(21)	Fe(1)	C(17)	C(19)	-119.96(18)	C(21) Fe(1) C(17) C(21) 0
C(17)	Fe(1)	C(22)	C(13)	165.5(2)	C(17) Fe(1) C(22) C(18) 46.3(3)
C(22)	Fe(1)	C(17)	C(19)	47.1(3)	C(22) Fe(1) C(17) C(21) 167.1(2)
C(18)	Fe(1)	C(19)	C(8)	121.72(13)	C(18) Fe(1) C(19) C(17) -118.57(13)
C(19)	Fe(1)	C(18)	C(20)	121.90(15)	C(19) Fe(1) C(18) C(22) -119.02(14)
C(18)	Fe(1)	C(20)	C(7)	-119.7(2)	C(18) Fe(1) C(20) C(18) 0
C(20)	Fe(1)	C(18)	C(20)	0	C(20) Fe(1) C(18) C(22) 119.1(2)
C(18)	Fe(1)	C(21)	C(12)	169.7(2)	C(18) Fe(1) C(21) C(17) 51.1(3)
C(21)	Fe(1)	C(18)	C(20)	42.3(3)	C(21) Fe(1) C(18) C(22) 161.4(2)

C(18)	Fe(1)	C(22)	C(13)	119.23(20)	C(18) Fe(1) C(22) C(18) 0
C(22)	Fe(1)	C(18)	C(20)	-119.1(2)	C(22) Fe(1) C(18) C(22) 0
C(19)	Fe(1)	C(20)	C(7)	161.96(14)	C(19) Fe(1) C(20) C(18) -78.36(18)
C(20)	Fe(1)	C(19)	C(8)	164.06(12)	C(20) Fe(1) C(19) C(17) -76.22(14)
C(19)	Fe(1)	C(21)	C(12)	81.57(13)	C(19) Fe(1) C(21) C(17) -37.10(13)
C(21)	Fe(1)	C(19)	C(8)	-82.45(13)	C(21) Fe(1) C(19) C(17) 37.27(12)
C(19)	Fe(1)	C(22)	C(13)	-160.01(14)	C(19) Fe(1) C(22) C(18) 80.76(15)
C(22)	Fe(1)	C(19)	C(8)	79.01(14)	C(22) Fe(1) C(19) C(17) -161.27(13)
C(20)	Fe(1)	C(21)	C(12)	-159.58(12)	C(20) Fe(1) C(21) C(17) 81.74(15)
C(21)	Fe(1)	C(20)	C(7)	78.02(17)	C(21) Fe(1) C(20) C(18) -162.31(15)
C(20)	Fe(1)	C(22)	C(13)	81.51(15)	C(20) Fe(1) C(22) C(18) -37.72(13)
C(22)	Fe(1)	C(20)	C(7)	-81.99(16)	C(22) Fe(1) C(20) C(18) 37.68(15)
C(21)	Fe(1)	C(22)	C(13)	-39.6(3)	C(21) Fe(1) C(22) C(18) -158.9(2)
C(22)	Fe(1)	C(21)	C(12)	-47.5(3)	C(22) Fe(1) C(21) C(17) -166.1(2)
C(4)	N(3)	C(6)	C(9)	-2.3(3)	C(4) N(3) C(6) C(11) 178.74(20)
C(6)	N(3)	C(4)	C(12)	179.02(18)	N(3) C(4) C(12) Fe(1) 95.6(2)
N(3)	C(4)	C(12)	C(8)	-175.1(2)	N(3) C(4) C(12) C(21) 7.3(3)
N(3)	C(6)	C(9)	N(5)	2(4)	N(3) C(6) C(11) N(2) 3.0(3)
N(3)	C(6)	C(11)	C(16)	-176.16(19)	C(9) C(6) C(11) N(2) -176.0(2)
C(9)	C(6)	C(11)	C(16)	4.9(3)	C(11) C(6) C(9) N(5) -179(3)
Fe(1)	C(7)	C(13)	Fe(1)	0	Fe(1) C(7) C(13) C(22) 59.87(19)
Fe(1)	C(7)	C(20)	Fe(1)	0	Fe(1) C(7) C(20) C(18) -59.50(17)
C(13)	C(7)	C(20)	Fe(1)	59.49(18)	C(13) C(7) C(20) C(18) -0.0(3)
C(20)	C(7)	C(13)	Fe(1)	-59.76(17)	C(20) C(7) C(13) C(22) 0.1(3)
Fe(1)	C(8)	C(12)	Fe(1)	0	Fe(1) C(8) C(12) C(4) -118.5(2)
Fe(1)	C(8)	C(12)	C(21)	59.44(15)	Fe(1) C(8) C(19) Fe(1) 0

Fe(1)	C(8)	C(19)	C(17)	-59.11(16)	C(12) C(8) C(19) Fe(1) 59.33(15)
C(12)	C(8)	C(19)	C(17)	0.2(3)	C(19) C(8) C(12) Fe(1) -60.02(15)
C(19)	C(8)	C(12)	C(4)	-178.5(2)	C(19) C(8) C(12) C(21) -0.6(2)
N(2)	C(11)	C(16)	N(15)	-58(3)	C(6) C(11) C(16) N(15) 121(3)
Fe(1)	C(12)	C(21)	Fe(1)	0	Fe(1) C(12) C(21) C(17) 60.23(16)
C(4)	C(12)	C(21)	Fe(1)	118.5(2)	C(4) C(12) C(21) C(17) 178.7(2)
C(8)	C(12)	C(21)	Fe(1)	-59.52(15)	C(8) C(12) C(21) C(17) 0.7(2)
Fe(1)	C(13)	C(22)	Fe(1)	0	Fe(1) C(13) C(22) C(18) 59.50(18)
C(7)	C(13)	C(22)	Fe(1)	-59.68(19)	C(7) C(13) C(22) C(18) -0.2(3)
Fe(1)	C(17)	C(19)	Fe(1)	0	Fe(1) C(17) C(19) C(8) 58.78(16)
Fe(1)	C(17)	C(21)	Fe(1)	0	Fe(1) C(17) C(21) C(12) -59.63(15)
C(19)	C(17)	C(21)	Fe(1)	59.05(17)	C(19) C(17) C(21) C(12) -0.6(3)
C(21)	C(17)	C(19)	Fe(1)	-58.56(17)	C(21) C(17) C(19) C(8) 0.2(3)
Fe(1)	C(18)	C(20)	Fe(1)	0	Fe(1) C(18) C(20) C(7) 59.18(16)
Fe(1)	C(18)	C(22)	Fe(1)	0	Fe(1) C(18) C(22) C(13) -59.01(18)
C(20)	C(18)	C(22)	Fe(1)	59.18(16)	C(20) C(18) C(22) C(13) 0.2(3)
C(22)	C(18)	C(20)	Fe(1)	-59.28(17)	C(22) C(18) C(20) C(7) -0.1(3)

Table 9. Possible hydrogen bonds

Donor	H	Acceptor	D...A	D-H	H...A	D-H...A
N(2)	H(24)	N(3)	2.767(2)	0.83	2.46(3)	103(2) intramol.
N(2)	H(26)	N(5)[1]	3.025(4)	0.81	2.254(15)	160(3)

Symmetry Operators:

(1) -X+2,Y+1/2-1,-Z+1/2+1

Table 10. Intramolecular contacts less than 3.60 Å

atom	atom	distance	atom	atom	distance
N(2)	N(3)	2.767(2)	N(2)	N(15)	3.391(4)
N(3)	N(5)	3.497(3)	N(3)	C(21)	2.921(3)
N(5)	C(4)	3.537(4)	N(5)	C(11)	3.522(3)
N(15)	C(6)	3.501(3)	N(15)	C(9)	3.587(2)
C(4)	C(9)	2.817(4)	C(4)	C(11)	3.553(2)
C(4)	C(13)	3.535(4)	C(9)	C(16)	2.8344(18)

Table 11. Intramolecular contacts less than 3.60 Å involving hydrogens

atom	atom	distance	atom	atom	distance
Fe(1)	H(4)	3.576	N(3)	H(21)	2.77(3)
N(3)	H(24)	2.460(20)	N(3)	H(26)	3.556(19)
N(5)	H(4)	2.910	N(15)	H(26)	3.30(3)
C(4)	H(8)	2.855(16)	C(4)	H(13)	3.22(5)
C(4)	H(21)	2.85(2)	C(6)	H(4)	2.513
C(6)	H(24)	2.54(2)	C(6)	H(26)	3.106(19)
C(7)	H(21)	3.37(5)	C(7)	H(22)	3.19(2)
C(7)	H(23)	3.21(2)	C(8)	H(4)	2.812
C(8)	H(17)	3.17(3)	C(8)	H(21)	3.235(17)
C(8)	H(22)	3.46(5)	C(9)	H(4)	2.465
C(12)	H(13)	3.34(5)	C(12)	H(17)	3.16(3)
C(12)	H(19)	3.22(2)	C(13)	H(14)	3.16(3)
C(13)	H(23)	3.21(3)	C(16)	H(24)	3.13(3)

C(16)	H(26)	2.47(3)	C(17)	H(8)	3.18(2)
C(17)	H(14)	3.43(4)	C(18)	H(10)	3.17(2)
C(18)	H(13)	3.14(4)	C(18)	H(19)	3.54(4)
C(19)	H(21)	3.235(15)	C(19)	H(23)	3.51(5)
C(20)	H(13)	3.13(4)	C(20)	H(17)	3.45(4)
C(20)	H(22)	3.19(2)	C(21)	H(4)	3.401
C(21)	H(8)	3.186(18)	C(21)	H(10)	3.35(5)
C(21)	H(19)	3.208(18)	C(22)	H(8)	3.43(5)
C(22)	H(10)	3.176(20)	C(22)	H(14)	3.17(2)
H(4)	H(8)	2.777	H(4)	H(13)	3.328
H(8)	H(19)	2.53(5)	H(8)	H(22)	3.32(5)
H(10)	H(13)	2.46(5)	H(10)	H(14)	2.45(5)
H(10)	H(21)	3.18(6)	H(13)	H(22)	2.46(4)
H(14)	H(17)	3.30(5)	H(14)	H(23)	2.51(2)
H(17)	H(19)	2.52(2)	H(17)	H(21)	2.49(5)
H(19)	H(23)	3.42(5)	H(21)	H(24)	3.42(4)
H(22)	H(23)	2.55(5)			

Table 12. Intermolecular contacts less than 3.60 Å

atom	atom	distance	atom	atom	distance
N(2)	N(5)^{1}	3.025(4)	N(2)	N(15)^{2}	3.134(6)
N(2)	C(4)^{3}	3.243(8)	N(2)	C(12)^{3}	3.474(9)
N(3)	N(3)^{3}	3.200(7)	N(3)	C(6)^{3}	3.266(7)
N(3)	C(11)^{3}	3.571(5)	N(5)	N(2)^{4}	3.025(6)
N(5)	C(7)^{5}	3.575(5)	N(15)	N(2)^{5}	3.134(3)

N(15)	C(17)[3]	3.522(10)	N(15)	C(19)[3]	3.404(10)
C(4)	N(2)[3]	3.243(8)	C(4)	C(6)[3]	3.484(8)
C(4)	C(11)[3]	3.269(7)	C(6)	N(3)[3]	3.266(7)
C(6)	C(4)[3]	3.484(8)	C(6)	C(17)[5]	3.586(6)
C(7)	N(5)[2]	3.575(6)	C(8)	C(16)[3]	3.385(9)
C(11)	N(3)[3]	3.571(5)	C(11)	C(4)[3]	3.269(7)
C(11)	C(12)[3]	3.205(9)	C(11)	C(21)[5]	3.379(5)
C(12)	N(2)[3]	3.474(9)	C(12)	C(11)[3]	3.205(9)
C(12)	C(16)[3]	3.323(7)	C(16)	C(8)[3]	3.385(9)
C(16)	C(12)[3]	3.323(7)	C(16)	C(19)[3]	3.562(10)
C(16)	C(21)[3]	3.481(9)	C(16)	C(21)[5]	3.478(6)
C(17)	N(15)[3]	3.522(10)	C(17)	C(6)[2]	3.586(6)
C(19)	N(15)[3]	3.404(9)	C(19)	C(16)[3]	3.562(10)
C(19)	C(19)[6]	3.481(5)	C(21)	C(11)[2]	3.379(5)
C(21)	C(16)[3]	3.481(9)	C(21)	C(16)[2]	3.478(5)

Symmetry Operators:

(1) -X+2,Y+1/2-1,-Z+1/2+1 (2) X,-Y+1/2+1,Z+1/2-1

(3) -X+2,-Y+2,-Z+1 (4) -X+2,Y+1/2,-Z+1/2+1

(5) X,-Y+1/2+1,Z+1/2 (6) -X+1,-Y+2,-Z

Table 13. Intermolecular contacts less than 3.60 Å involving hydrogens

atom	atom	distance	atom	atom	distance
Fe(1)	H(13)[1]	3.57(3)	Fe(1)	H(19)[2]	3.412(16)

N(2)	H(4)^{3}	3.196	N(2)	H(17)^{4}	3.37(3)
N(2)	H(21)^{4}	3.24(3)	N(2)	H(22)^{5}	3.43(6)
N(3)	H(17)^{4}	2.85(3)	N(5)	H(10)^{4}	2.98(3)
N(5)	H(14)^{4}	3.153(14)	N(5)	H(22)^{6}	2.87(3)
N(5)	H(23)^{7}	3.05(5)	N(5)	H(24)^{8}	3.470(18)
N(5)	H(26)^{8}	2.254(18)	N(15)	H(21)^{4}	2.923(13)
N(15)	H(23)^{9}	3.39(3)	N(15)	H(24)^{4}	2.40(4)
N(15)	H(26)^{4}	3.28(3)	C(4)	H(17)^{4}	3.44(4)
C(4)	H(24)^{3}	3.40(6)	C(6)	H(17)^{4}	2.98(2)
C(6)	H(21)^{4}	3.21(3)	C(7)	H(8)^{10}	2.92(3)
C(7)	H(17)^{4}	3.38(2)	C(7)	H(19)^{4}	3.14(3)
C(7)	H(22)^{10}	3.38(3)	C(8)	H(19)^{2}	2.88(4)
C(8)	H(23)^{2}	3.25(3)	C(9)	H(10)^{4}	3.22(3)
C(9)	H(14)^{4}	3.18(2)	C(9)	H(21)^{3}	3.49(6)
C(9)	H(26)^{8}	3.12(3)	C(11)	H(4)^{3}	3.597
C(11)	H(17)^{4}	3.191(15)	C(11)	H(21)^{4}	2.71(2)
C(13)	H(8)^{10}	2.71(2)	C(13)	H(14)^{4}	3.53(2)
C(13)	H(17)^{4}	3.28(4)	C(13)	H(19)^{4}	3.26(4)
C(13)	H(23)^{4}	3.40(3)	C(16)	H(21)^{4}	2.565(17)
C(16)	H(24)^{4}	3.33(3)	C(17)	H(10)^{1}	3.40(3)
C(17)	H(13)^{1}	3.13(2)	C(18)	H(4)^{10}	3.180
C(18)	H(13)^{1}	3.19(3)	C(18)	H(19)^{2}	3.25(3)
C(19)	H(8)^{2}	3.29(4)	C(19)	H(10)^{1}	3.35(2)
C(19)	H(13)^{1}	3.28(2)	C(19)	H(19)^{2}	2.94(3)
C(19)	H(22)^{2}	3.530(20)	C(19)	H(23)^{2}	3.31(3)
C(20)	H(4)^{10}	3.287	C(20)	H(8)^{10}	3.51(2)

C(20)	H(13)[1]	3.12(4)	C(20)	H(14)[11]	3.51(5)
C(22)	H(8)[10]	3.23(3)	C(22)	H(19)[2]	3.13(2)
C(22)	H(26)[12]	3.29(4)	H(4)	N(2)[3]	3.196
H(4)	C(11)[3]	3.597	H(4)	C(18)[7]	3.180
H(4)	C(20)[7]	3.287	H(4)	H(14)[7]	3.502
H(4)	H(14)[4]	3.129	H(4)	H(23)[7]	3.302
H(4)	H(24)[3]	3.241	H(4)	H(26)[3]	3.540
H(8)	C(7)[7]	2.92(3)	H(8)	C(13)[7]	2.71(3)
H(8)	C(19)[2]	3.29(6)	H(8)	C(20)[7]	3.51(3)
H(8)	C(22)[7]	3.23(5)	H(8)	H(10)[7]	3.21(7)
H(8)	H(13)[7]	2.86(5)	H(8)	H(19)[2]	2.49(11)
H(8)	H(23)[2]	2.91(5)	H(8)	H(26)[3]	3.48(13)
H(10)	N(5)[1]	2.98(4)	H(10)	C(9)[1]	3.22(3)
H(10)	C(17)[4]	3.40(6)	H(10)	C(19)[4]	3.35(3)
H(10)	H(8)[10]	3.21(8)	H(10)	H(17)[4]	2.95(7)
H(10)	H(19)[4]	2.77(4)	H(10)	H(22)[10]	2.88(6)
H(13)	Fe(1)[4]	3.57(5)	H(13)	C(17)[4]	3.13(5)
H(13)	C(18)[4]	3.19(4)	H(13)	C(19)[4]	3.28(2)
H(13)	C(20)[4]	3.12(7)	H(13)	H(8)[10]	2.86(9)
H(13)	H(14)[4]	2.71(9)	H(13)	H(17)[4]	2.72(4)
H(13)	H(19)[4]	2.98(6)	H(13)	H(23)[4]	2.84(5)
H(14)	N(5)[1]	3.153(16)	H(14)	C(9)[1]	3.18(3)
H(14)	C(13)[1]	3.53(2)	H(14)	C(20)[11]	3.51(8)
H(14)	H(4)[10]	3.502	H(14)	H(4)[1]	3.129
H(14)	H(13)[1]	2.71(4)	H(14)	H(14)[11]	2.90(9)
H(17)	N(2)[1]	3.37(4)	H(17)	N(3)[1]	2.85(5)

H(17)	C(4)[1]	3.44(7)	H(17)	C(6)[1]	2.98(3)
H(17)	C(7)[1]	3.38(5)	H(17)	C(11)[1]	3.19(2)
H(17)	C(13)[1]	3.28(7)	H(17)	H(10)[1]	2.95(3)
H(17)	H(13)[1]	2.72(6)	H(17)	H(24)[1]	3.15(5)
H(19)	Fe(1)[2]	3.412(18)	H(19)	C(7)[1]	3.14(6)
H(19)	C(8)[2]	2.88(6)	H(19)	C(13)[1]	3.26(7)
H(19)	C(18)[2]	3.25(4)	H(19)	C(19)[2]	2.94(4)
H(19)	C(22)[2]	3.13(2)	H(19)	H(8)[2]	2.49(11)
H(19)	H(10)[1]	2.77(6)	H(19)	H(13)[1]	2.98(9)
H(19)	H(19)[2]	2.63(7)	H(19)	H(22)[2]	2.77(4)
H(19)	H(23)[2]	2.98(9)	H(21)	N(2)[1]	3.24(3)
H(21)	N(15)[1]	2.923(16)	H(21)	C(6)[1]	3.21(6)
H(21)	C(9)[3]	3.49(9)	H(21)	C(11)[1]	2.71(4)
H(21)	C(16)[1]	2.56(2)	H(21)	H(26)[1]	3.27(5)
H(22)	N(2)[12]	3.43(8)	H(22)	N(5)[6]	2.87(3)
H(22)	C(7)[7]	3.38(6)	H(22)	C(19)[2]	3.53(2)
H(22)	H(10)[7]	2.88(3)	H(22)	H(19)[2]	2.77(4)
H(22)	H(24)[12]	3.55(7)	H(22)	H(26)[12]	2.87(6)
H(23)	N(5)[10]	3.05(9)	H(23)	N(15)[13]	3.39(4)
H(23)	C(8)[2]	3.25(3)	H(23)	C(13)[1]	3.40(3)
H(23)	C(19)[2]	3.31(5)	H(23)	H(4)[10]	3.302
H(23)	H(8)[2]	2.91(4)	H(23)	H(13)[1]	2.84(5)
H(23)	H(19)[2]	2.98(9)	H(24)	N(5)[14]	3.47(3)
H(24)	N(15)[1]	2.40(7)	H(24)	C(4)[3]	3.40(8)
H(24)	C(16)[1]	3.33(7)	H(24)	H(4)[3]	3.241
H(24)	H(17)[4]	3.15(5)	H(24)	H(22)[5]	3.55(4)

H(26)	N(5)^{14}	2.25(2)	H(26)	N(15)^{1}	3.28(7)
H(26)	C(9)^{14}	3.12(4)	H(26)	C(22)^{5}	3.29(4)
H(26)	H(4)^{3}	3.540	H(26)	H(8)^{3}	3.48(14)
H(26)	H(21)^{4}	3.27(5)	H(26)	H(22)^{5}	2.87(6)

Symmetry Operators:

(1) X,-Y+1/2+1,Z+1/2-1	(2) -X+1,-Y+2,-Z
(3) -X+2,-Y+2,-Z+1	(4) X,-Y+1/2+1,Z+1/2
(5) X+1,-Y+1/2+1,Z+1/2	(6) -X+1,-Y+2,-Z+1
(7) -X+1,Y+1/2,-Z+1/2	(8) -X+2,Y+1/2,-Z+1/2+1
(9) X+1,Y,Z+1	(10) -X+1,Y+1/2-1,-Z+1/2
(11) -X+1,-Y+1,-Z	(12) X-1,-Y+1/2+1,Z+1/2-1
(13) X-1,Y,Z-1	(14) -X+2,Y+1/2-1,-Z+1/2+1

6.2 CIF file for 2

data_global
_audit_creation_date "10-02-22"
_audit_creation_method CRYSTALS_ver_14.05

_oxford_structure_analysis_title 'Fc2DAMN in P2(1)/n'

_publ_section_exptl_refinement
Some potentially useful phrases are donated by Bill Clegg:
In the absence of significant anomalous scattering, Friedel pairs were merged.

The absolute configuration was arbitrarily assigned.

The relatively large ratio of minimum to maximum corrections applied in the multiscan process (1:nnn) reflect changes in the illuminated volume of the crystal.

Changes in illuminated volume were kept to a minimum, and were taken into account (G\"orbitz, 1999) by the multi-scan inter-frame scaling (DENZO/SCALEPACK, Otwinowski & Minor, 1997).

G\"orbitz, C. H. (1999). Acta Cryst. B55, 1090-1098.

The H atoms were all located in a difference map, but those attached to carbon atoms were repositioned geometrically.
The H atoms were initially refined with soft restraints on the bond lengths and angles to regularise their geometry
(C---H in the range 0.93--0.98,
N---H in the range 0.86--0.89
N---H to 0.86
O---H = 0.82
\%A)
and
U~iso~(H) (in the range 1.2-1.5 times U~eq~ of the parent atom),
after which the positions were refined with riding constraints.

data_1

_exptl_special_details

The crystal was
placed in the cold stream of an Oxford

Cryosystems open-flow nitrogen cryostat (Cosier &
Glazer, 1986) with a nominal stability of 0.1K.

Cosier, J. & Glazer, A.M., 1986. J. Appl. Cryst. 105 107.

_refine_special_details

_cell_length_a 5.9178(12)
_cell_length_b 21.699(4)
_cell_length_c 8.4626(17)
_cell_angle_alpha 90
_cell_angle_beta 95.54(3)
_cell_angle_gamma 90
_cell_volume 1081.6(4)

_symmetry_cell_setting 'Monoclinic'
_symmetry_space_group_name_H-M 'P 1 21/n 1 '
_symmetry_space_group_name_Hall ?
loop_
_symmetry_equiv_pos_as_xyz
'x,y,z'
'-x,-y,-z'
'-x+1/2,y+1/2,-z+1/2'
'x+1/2,-y+1/2,z+1/2'

loop_
_atom_type_symbol
_atom_type_scat_dispersion_real
_atom_type_scat_dispersion_imag
_atom_type_scat_Cromer_Mann_a1
_atom_type_scat_Cromer_Mann_b1
_atom_type_scat_Cromer_Mann_a2
_atom_type_scat_Cromer_Mann_b2
_atom_type_scat_Cromer_Mann_a3
_atom_type_scat_Cromer_Mann_b3
_atom_type_scat_Cromer_Mann_a4
_atom_type_scat_Cromer_Mann_b4
_atom_type_scat_Cromer_Mann_c
_atom_type_scat_source
C 0.0033 0.0016 2.3100 20.8439 1.0200 10.2075 1.5886 0.5687
0.8650 51.6512 0.2156 'International Tables Vol C 4.2.6.8 and 6.1.1.4'
H 0.0000 0.0000 0.4930 10.5109 0.3229 26.1257 0.1402 3.1424
0.0408 57.7998 0.0030 'International Tables Vol C 4.2.6.8 and 6.1.1.4'
N 0.0061 0.0033 12.2126 0.0057 3.1322 9.8933 2.0125 28.9975

```
  1.1663   0.5826 -11.5290 'International Tables Vol C 4.2.6.8 and 6.1.1.4'
Fe      0.3463   0.8444  11.7695   4.7611   7.3573   0.3072   3.5222  15.3535
  2.3045  76.8805   1.0369 'International Tables Vol C 4.2.6.8 and 6.1.1.4'


_cell_formula_units_Z                2

# Given Formula = C26 H20 Fe2 N4
# Dc =      1.54 Fooo =    512.00 Mu =     13.63 M =    250.08
# Found Formula = C26 H20 Fe2 N4
# Dc =      1.54 FOOO =    512.00 Mu =     13.63 M =    250.08

_chemical_formula_sum           'C26 H20 Fe2 N4'
_chemical_formula_moiety         'C26 H20 Fe2 N4'
_chemical_compound_source              ?
_chemical_formula_weight          500.17


_cell_measurement_reflns_used          25
_cell_measurement_theta_min            15
_cell_measurement_theta_max            18
_cell_measurement_temperature         298

_exptl_crystal_description       'plate'
_exptl_crystal_colour           'blur'
_exptl_crystal_size_min          0.050
_exptl_crystal_size_mid          0.150
_exptl_crystal_size_max          0.350

_exptl_crystal_density_diffrn     1.536
_exptl_crystal_density_meas       ?
_exptl_crystal_density_method     'not measured'
# Non-dispersive F(000):
_exptl_crystal_F_000            512
_exptl_absorpt_coefficient_mu     1.363

# Sheldrick geometric approximatio 0.82 0.93
_exptl_absorpt_correction_type    psi-scan
_exptl_absorpt_process_details    '(North et al., 1968)'
_exptl_absorpt_correction_T_min   0.78
_exptl_absorpt_correction_T_max   0.93
_diffrn_measurement_device_type   'Unknown'
_diffrn_measurement_device        'Serial'
_diffrn_radiation_monochromator   'graphite'
```

```
_diffrn_radiation_type          'Mo K\a'
_diffrn_radiation_wavelength          0.71073
_diffrn_measurement_method       \w/2\q

# If a reference occurs more than once, delete the author
# and date from subsequent references.
_computing_data_collection       'USER DEFINED DATA COLLECTION'
_computing_cell_refinement       'USER DEFINED CELL REFINEMENT'
_computing_data_reduction        'USER DEFINED DATA REDUCTION'
_computing_structure_solution    'SIR92 (Altomare et al., 1994)'
_computing_structure_refinement  'CRYSTALS (Betteridge et al., 2003)'
_computing_publication_material  'CRYSTALS (Betteridge et al., 2003)'
_computing_molecular_graphics    'CAMERON (Watkin et al., 1996)'

_diffrn_standards_interval_time   .
_diffrn_standards_interval_count  150
_diffrn_standards_number          3
_diffrn_standards_decay_%         0.00

_diffrn_ambient_temperature       298
_diffrn_reflns_number             2560
_reflns_number_total              2483
_diffrn_reflns_av_R_equivalents   0.000
# Number of reflections without Friedels Law is 2483
# Number of reflections with Friedels Law is 0
# Theoretical number of reflections is about 2486


_diffrn_reflns_theta_min          2.594
_diffrn_reflns_theta_max          27.505
_diffrn_measured_fraction_theta_max 0.999

_diffrn_reflns_theta_full         27.505
_diffrn_measured_fraction_theta_full 0.999


_diffrn_reflns_limit_h_min        -7
_diffrn_reflns_limit_h_max        7
_diffrn_reflns_limit_k_min        -28
_diffrn_reflns_limit_k_max        0
_diffrn_reflns_limit_l_min        -10
_diffrn_reflns_limit_l_max        0
_reflns_limit_h_min               -7
_reflns_limit_h_max               7
```

```
_reflns_limit_k_min              0
_reflns_limit_k_max              28
_reflns_limit_l_min              0
_reflns_limit_l_max              10

_oxford_diffrn_Wilson_B_factor    3.11
_oxford_diffrn_Wilson_scale       6.31

_atom_sites_solution_primary      direct #heavy,direct,difmap,geom
# _atom_sites_solution_secondary  difmap
_atom_sites_solution_hydrogens    geom

_refine_diff_density_min         -0.34
_refine_diff_density_max          0.44


# The current dictionary definitions do not cover the
# situation where the reflections used for refinement were
# selected by a user-defined sigma threshold


# The values actually used during refinement
_oxford_reflns_threshold_expression_ref     I>3.0\s(I)
_refine_ls_number_reflns          1638
_refine_ls_number_restraints      0
_refine_ls_number_parameters      145
_oxford_refine_ls_R_factor_ref    0.0455
_refine_ls_wR_factor_ref          0.1124
_refine_ls_goodness_of_fit_ref    1.0052
_refine_ls_shift/su_max           0.0005762
_refine_ls_shift/su_mean          0.0000852


# The values computed from all data
_oxford_reflns_number_all         2476
_refine_ls_R_factor_all           0.0828
_refine_ls_wR_factor_all          0.1343

# The values computed with a 2 sigma cutoff - a la SHELX
_reflns_threshold_expression      I>2.0\s(I)
_reflns_number_gt                 1680
_refine_ls_R_factor_gt            0.0463
_refine_ls_wR_factor_gt           0.1137
```

```
# choose from: rm (reference molecule of known chirality),
# ad (anomolous dispersion - Flack), rmad (rm and ad),
# syn (from synthesis), unk (unknown) or . (not applicable).
_chemical_absolute_configuration  '.'


_refine_ls_structure_factor_coef  Fsqd
_refine_ls_matrix_type            full
_refine_ls_hydrogen_treatment     none          # none, undef, noref, refall,
                                  # refxyz, refU, constr or mixed
_refine_ls_weighting_scheme       calc
_refine_ls_weighting_details

 Method= Modified Sheldrick
 w=1/[\s^2^(F^2^) + ( 0.07P)^2^ + 0.45P]
 ,where P=(max(Fo^2^,0) + 2Fc^2^)/3

# Insert your own references if required - in alphabetical order
_publ_section_references

User-defined data collection reference

User defined data reduction

User defined cell refinement

Altomare, A., Cascarano, G., Giacovazzo, C., Guagliardi, A., Burla, M.C.,
Polidori, G. & Camalli, M. (1994). J. Appl. Cryst. 27, 435.

Betteridge, P.W., Carruthers, J.R., Cooper, R.I.,
Prout, K. & Watkin, D.J. (2003). J. Appl. Cryst. 36, 1487.

North, A.C.T., Phillips, D.C. & Mathews, F.S., (1968).
Acta Cryst, A24, 351-359.

Watkin, D.J., Prout, C.K. & Pearce, L.J. (1996). CAMERON, Chemical
Crystallography Laboratory, Oxford, UK.


# Uequiv = arithmetic mean of Ui i.e. Ueqiv = (U1+U2+U3)/3

# Replace last . with number of unfound hydrogen atomsattached to an atom.

# ..._refinement_flags_...
```

. no refinement constraints S special position constraint on site
G rigid group refinement of site R riding atom
D distance or angle restraint on site T thermal displacement constraints
U Uiso or Uij restraint (rigid bond) P partial occupancy constraint

loop_
_atom_site_label
_atom_site_type_symbol
_atom_site_fract_x
_atom_site_fract_y
_atom_site_fract_z
_atom_site_U_iso_or_equiv
_atom_site_occupancy
_atom_site_adp_type
_atom_site_refinement_flags_posn
_atom_site_refinement_flags_adp
_atom_site_refinement_flags_occupancy
_atom_site_disorder_assembly
_atom_site_disorder_group
_oxford_atom_site_special_shape
_atom_site_attached_hydrogens
Fe1 Fe 0.23627(9) 0.34383(2) 0.05106(6) 0.0399 1.0000 Uani . . . . . .
C2 C 0.1434(7) 0.43382(17) 0.0552(4) 0.0430 1.0000 Uani . . . . . .
C3 C -0.0451(7) 0.39653(19) 0.0012(5) 0.0506 1.0000 Uani . . . . . .
C4 C 0.0049(9) 0.3658(2) -0.1372(5) 0.0619 1.0000 Uani . . . . . .
C5 C 0.2243(9) 0.3832(2) -0.1707(5) 0.0624 1.0000 Uani . . . . . .
C6 C 0.3112(7) 0.42503(19) -0.0537(5) 0.0503 1.0000 Uani . . . . . .
C7 C 0.1779(7) 0.46805(18) 0.2020(5) 0.0479 1.0000 Uani . . . . . .
N8 N 0.0266(6) 0.46870(15) 0.3021(4) 0.0477 1.0000 Uani . . . . . .
C9 C 0.0691(8) 0.5028(2) 0.4417(5) 0.0505 1.0000 Uani . . . . . .
C10 C 0.2538(8) 0.5461(2) 0.4635(5) 0.0547 1.0000 Uani . . . . . .
N11 N 0.4020(8) 0.5794(2) 0.4684(5) 0.0779 1.0000 Uani . . . . . .
C12 C 0.2964(10) 0.2512(2) 0.0617(6) 0.0694 1.0000 Uani . . . . . .
C13 C 0.1555(9) 0.2696(3) 0.1819(8) 0.0777 1.0000 Uani . . . . . .
C14 C 0.2872(10) 0.3124(2) 0.2781(5) 0.0648 1.0000 Uani . . . . . .
C15 C 0.4917(9) 0.3202(2) 0.2183(5) 0.0616 1.0000 Uani . . . . . .
C16 C 0.4994(9) 0.2831(2) 0.0881(6) 0.0617 1.0000 Uani . . . . . .
H31 H -0.1896 0.3948 0.0529 0.0608 1.0000 Uiso R . . . . . .
H41 H -0.0996 0.3378 -0.1996 0.0736 1.0000 Uiso R . . . . . .
H51 H 0.3008 0.3685 -0.2619 0.0755 1.0000 Uiso R . . . . . .
H61 H 0.4638 0.4444 -0.0435 0.0630 1.0000 Uiso R . . . . . .
H71 H 0.3190 0.4907 0.2233 0.0601 1.0000 Uiso R . . . . . .
H121 H 0.2587 0.2222 -0.0252 0.0808 1.0000 Uiso R . . . . . .

H141 H 0.2348 0.3350 0.3678 0.0771 1.0000 Uiso R . . . . . .
H151 H 0.6134 0.3475 0.2634 0.0735 1.0000 Uiso R . . . . . .
H161 H 0.6237 0.2824 0.0171 0.0750 1.0000 Uiso R . . . . . .
H7 H 0.0078 0.2541 0.1972 0.0916 1.0000 Uiso R . . . . . .
loop_
_atom_site_aniso_label
_atom_site_aniso_U_11
_atom_site_aniso_U_22
_atom_site_aniso_U_33
_atom_site_aniso_U_23
_atom_site_aniso_U_13
_atom_site_aniso_U_12
Fe1 0.0447(3) 0.0383(3) 0.0366(3) 0.0014(2) 0.0039(2) 0.0019(3)
C2 0.050(2) 0.039(2) 0.040(2) 0.0050(16) 0.0042(17) 0.0069(18)
C3 0.045(2) 0.055(3) 0.051(2) 0.007(2) 0.0007(19) 0.0023(19)
C4 0.082(3) 0.051(3) 0.048(3) 0.002(2) -0.019(2) 0.001(2)
C5 0.095(4) 0.057(3) 0.037(2) 0.007(2) 0.019(2) 0.013(3)
C6 0.053(3) 0.046(2) 0.054(3) 0.011(2) 0.013(2) -0.0017(18)
C7 0.054(2) 0.040(2) 0.049(2) 0.0010(18) 0.0015(19) 0.0018(19)
N8 0.056(2) 0.0448(19) 0.0424(18) -0.0014(15) 0.0078(15) 0.0051(16)
C9 0.062(3) 0.043(2) 0.046(2) -0.0012(18) 0.0054(19) 0.007(2)
C10 0.064(3) 0.054(3) 0.047(2) -0.008(2) 0.006(2) -0.002(2)
N11 0.085(3) 0.080(3) 0.070(3) -0.017(2) 0.012(2) -0.024(3)
C12 0.102(4) 0.034(2) 0.065(3) 0.002(2) -0.025(3) 0.005(2)
C13 0.052(3) 0.074(4) 0.107(4) 0.053(3) 0.006(3) -0.002(3)
C14 0.089(4) 0.061(3) 0.046(3) 0.015(2) 0.015(2) 0.015(3)
C15 0.074(3) 0.058(3) 0.049(3) 0.004(2) -0.012(2) 0.005(2)
C16 0.062(3) 0.058(3) 0.064(3) 0.003(2) 0.003(2) 0.012(2)

_refine_ls_extinction_method
'None'
_oxford_refine_ls_scale 0.4092(10)
loop_
_geom_bond_atom_site_label_1
_geom_bond_site_symmetry_1
_geom_bond_atom_site_label_2
_geom_bond_site_symmetry_2
_geom_bond_distance
_geom_bond_publ_flag
Fe1 . C2 . 2.030(4) yes
Fe1 . C3 . 2.030(4) yes
Fe1 . C4 . 2.054(4) yes
Fe1 . C5 . 2.057(4) yes
Fe1 . C6 . 2.040(4) yes

```
Fe1 . C12 . 2.042(4)    yes
Fe1 . C13 . 2.037(5)    yes
Fe1 . C14 . 2.034(4)    yes
Fe1 . C15 . 2.034(4)    yes
Fe1 . C16 . 2.040(5)    yes
C2 . C3 . 1.417(6)    yes
C2 . C6 . 1.431(5)    yes
C2 . C7 . 1.445(5)    yes
C3 . C4 . 1.404(6)    yes
C3 . H31 . 0.998    no
C4 . C5 . 1.407(7)    yes
C4 . H41 . 0.984    no
C5 . C6 . 1.404(6)    yes
C5 . H51 . 0.985    no
C6 . H61 . 0.992    no
C7 . N8 . 1.290(5)    yes
C7 . H71 . 0.971    no
N8 . C9 . 1.396(5)    yes
C9 . C9 2_566 1.347(8)    yes
C9 . C10 . 1.440(6)    yes
C10 . N11 . 1.134(6)    yes
C12 . C13 . 1.433(7)    yes
C12 . C16 . 1.386(7)    yes
C12 . H121 . 0.977    no
C13 . C14 . 1.418(8)    yes
C13 . H7 . 0.957    no
C14 . C15 . 1.367(7)    yes
C14 . H141 . 0.978    no
C15 . C16 . 1.369(7)    yes
C15 . H151 . 0.981    no
C16 . H161 . 0.993    no
loop_
 _geom_angle_atom_site_label_1
 _geom_angle_site_symmetry_1
 _geom_angle_atom_site_label_2
 _geom_angle_site_symmetry_2
 _geom_angle_atom_site_label_3
 _geom_angle_site_symmetry_3
 _geom_angle
 _geom_angle_publ_flag
C2 . Fe1 . C3 . 40.87(16)    yes
C2 . Fe1 . C4 . 68.20(17)    yes
C3 . Fe1 . C4 . 40.21(18)    yes
C2 . Fe1 . C5 . 68.33(17)    yes
```

C3 . Fe1 . C5 . 67.75(18) yes
C4 . Fe1 . C5 . 40.02(19) yes
C2 . Fe1 . C6 . 41.17(15) yes
C3 . Fe1 . C6 . 68.39(17) yes
C4 . Fe1 . C6 . 67.61(19) yes
C5 . Fe1 . C6 . 40.08(17) yes
C2 . Fe1 . C12 . 173.0(2) yes
C3 . Fe1 . C12 . 134.4(2) yes
C4 . Fe1 . C12 . 111.30(19) yes
C5 . Fe1 . C12 . 116.1(2) yes
C6 . Fe1 . C12 . 145.6(2) yes
C2 . Fe1 . C13 . 132.3(2) yes
C3 . Fe1 . C13 . 109.11(19) yes
C4 . Fe1 . C13 . 115.6(2) yes
C5 . Fe1 . C13 . 146.6(2) yes
C6 . Fe1 . C13 . 172.3(2) yes
C2 . Fe1 . C14 . 108.75(18) yes
C3 . Fe1 . C14 . 115.4(2) yes
C4 . Fe1 . C14 . 146.9(2) yes
C5 . Fe1 . C14 . 171.9(2) yes
C6 . Fe1 . C14 . 132.9(2) yes
C2 . Fe1 . C15 . 114.52(18) yes
C3 . Fe1 . C15 . 145.7(2) yes
C4 . Fe1 . C15 . 173.3(2) yes
C5 . Fe1 . C15 . 134.2(2) yes
C6 . Fe1 . C15 . 110.0(2) yes
C2 . Fe1 . C16 . 145.30(19) yes
C3 . Fe1 . C16 . 173.63(19) yes
C4 . Fe1 . C16 . 135.3(2) yes
C5 . Fe1 . C16 . 111.5(2) yes
C6 . Fe1 . C16 . 115.43(19) yes
C12 . Fe1 . C13 . 41.2(2) yes
C12 . Fe1 . C14 . 67.6(2) yes
C13 . Fe1 . C14 . 40.8(2) yes
C12 . Fe1 . C15 . 66.8(2) yes
C13 . Fe1 . C15 . 67.7(2) yes
C14 . Fe1 . C15 . 39.3(2) yes
C12 . Fe1 . C16 . 39.7(2) yes
C13 . Fe1 . C16 . 67.8(2) yes
C14 . Fe1 . C16 . 66.3(2) yes
C15 . Fe1 . C16 . 39.25(19) yes
Fe1 . C2 . C3 . 69.6(2) yes
Fe1 . C2 . C6 . 69.8(2) yes
C3 . C2 . C6 . 106.9(4) yes

Fe1 . C2 . C7 . 119.6(3) yes
C3 . C2 . C7 . 127.7(4) yes
C6 . C2 . C7 . 124.9(4) yes
C2 . C3 . Fe1 . 69.5(2) yes
C2 . C3 . C4 . 108.5(4) yes
Fe1 . C3 . C4 . 70.8(3) yes
C2 . C3 . H31 . 124.2 no
Fe1 . C3 . H31 . 127.5 no
C4 . C3 . H31 . 127.3 no
C3 . C4 . Fe1 . 69.0(2) yes
C3 . C4 . C5 . 108.3(4) yes
Fe1 . C4 . C5 . 70.1(3) yes
C3 . C4 . H41 . 124.7 no
Fe1 . C4 . H41 . 127.6 no
C5 . C4 . H41 . 127.0 no
C4 . C5 . Fe1 . 69.9(2) yes
C4 . C5 . C6 . 108.3(4) yes
Fe1 . C5 . C6 . 69.3(2) yes
C4 . C5 . H51 . 125.0 no
Fe1 . C5 . H51 . 127.1 no
C6 . C5 . H51 . 126.7 no
C2 . C6 . C5 . 108.1(4) yes
C2 . C6 . Fe1 . 69.0(2) yes
C5 . C6 . Fe1 . 70.6(2) yes
C2 . C6 . H61 . 124.8 no
C5 . C6 . H61 . 127.1 no
Fe1 . C6 . H61 . 124.2 no
C2 . C7 . N8 . 121.4(4) yes
C2 . C7 . H71 . 117.9 no
N8 . C7 . H71 . 120.8 no
C7 . N8 . C9 . 118.8(4) yes
N8 . C9 . C9 2_566 120.0(5) yes
N8 . C9 . C10 . 121.8(3) yes
C9 2_566 C9 . C10 . 118.1(5) yes
C9 . C10 . N11 . 174.5(5) yes
Fe1 . C12 . C13 . 69.2(3) yes
Fe1 . C12 . C16 . 70.1(3) yes
C13 . C12 . C16 . 107.5(4) yes
Fe1 . C12 . H121 . 125.0 no
C13 . C12 . H121 . 127.4 no
C16 . C12 . H121 . 125.1 no
C12 . C13 . Fe1 . 69.6(3) yes
C12 . C13 . C14 . 105.4(4) yes
Fe1 . C13 . C14 . 69.5(3) yes

C12 . C13 . H7 . 126.8 no
Fe1 . C13 . H7 . 128.1 no
C14 . C13 . H7 . 127.7 no
C13 . C14 . Fe1 . 69.7(3) yes
C13 . C14 . C15 . 109.0(5) yes
Fe1 . C14 . C15 . 70.4(3) yes
C13 . C14 . H141 . 125.1 no
Fe1 . C14 . H141 . 122.4 no
C15 . C14 . H141 . 125.8 no
Fe1 . C15 . C14 . 70.3(3) yes
Fe1 . C15 . C16 . 70.6(3) yes
C14 . C15 . C16 . 109.0(5) yes
Fe1 . C15 . H151 . 125.9 no
C14 . C15 . H151 . 125.0 no
C16 . C15 . H151 . 126.0 no
C12 . C16 . Fe1 . 70.2(3) yes
C12 . C16 . C15 . 109.1(5) yes
Fe1 . C16 . C15 . 70.1(3) yes
C12 . C16 . H161 . 125.1 no
Fe1 . C16 . H161 . 121.1 no
C15 . C16 . H161 . 125.5 no